Copy 196

RM A54H09

NACA

RESEARCH MEMORANDUM

EXPERIMENTAL AND PREDICTED LONGITUDINAL RESPONSE CHARACTERISTICS OF A LARGE FLEXIBLE 35° SWEPT-WING AIRPLANE AT AN ALTITUDE OF 35,000 FEET

By Henry A. Cole, Jr., Stuart C. Brown, and Euclid C. Holleman

Ames Aeronautical Laboratory
Moffett Field, Calif.

NATIONAL ADVISORY COMMITTEE FOR AERONAUTICS

WASHINGTON

November 26, 1954

NATIONAL ADVISORY COMMITTEE FOR AERONAUTICS

RESEARCH MEMORANDUM

EXPERIMENTAL AND PREDICTED LONGITUDINAL RESPONSE CHARACTERISTICS OF A LARGE FLEXIBLE 35° SWEPT-WING AIRPLANE AT AN ALTITUDE OF 35,000 FEET

By Henry A. Cole, Jr., Stuart C. Brown, and Euclid C. Holleman

SUMMARY

The longitudinal frequency response of a large flexible swept-wing airplane as determined from transient flight data, excited by elevator pulses, is presented for flight conditions of 0.6 to 0.85 Mach number at an altitude of 35,000 feet for a range of center-of-gravity locations. These data cover a band of frequencies which include the short-period mode and two aeroelastic modes. Response quantities are presented for center-of-gravity, wing, and tail locations in order to define the mode shapes.

Predicted transfer functions based on the two-degree-of-freedom longitudinal equations of motion, with coefficients modified to include flexibility effects, are compared with experimental transfer functions evaluated from the measured frequency responses. Comparisons are also made with transfer functions predicted for the rigid airplane in order to show the effects of flexibility. The results are presented in the form of transfer-function coefficients for the response of the center of gravity and show good agreement between predicted and experimental values, except at conditions where the airplane has a pitch-up tendency. For responses near the wing tip, this theory becomes inadequate for frequences near and above the wing first-bending mode frequency.

A method for determining the aerodynamic lift and moment of a flexible wing through use of aerodynamic and structural influence coefficients is presented.

INTRODUCTION

The desire to increase the range and speed of large airplanes has recently led to configurations with sweptback wings of high aspect ratio, thin airfoils, and fuselages of high fineness ratio. All of these factors

tend to increase the flexibility of the structure, and the associated aeroelastic effects are becoming of greater importance in problems of static and dynamic stability and control. The dynamic effects are especially important when the airplane is equipped with automatic control because structural modes may introduce system instabilities which would not be present in a rigid airplane. It is important to be able to predict these aeroelastic effects in order to insure that the basic handling qualities and loads requirements are satisfied, and to permit rational design of automatic control systems concurrently with the airplane.

In view of the above problems, the NACA is currently flight testing a large flexible 35° swept-wing airplane over its entire operating range of Mach numbers and dynamic pressures. The aims of this program are to document and analyze the airplane response to control surface motions and, through comparisons between measured and predicted response characteristics, to establish simple but adequate methods of prediction for flexible airplanes. The flight data considered in the present report consist of measurements of longitudinal response to elevator deflection at an altitude of 35,000 feet over a Mach number range of 0.6 to 0.85 for several center-of-gravity positions. The measured response quantities (normal acceleration at several stations, pitching velocity at the center of gravity, and wing deflections) were suitable for frequency-response analysis over a range of frequencies including the short-period longitudinal mode and the first two aeroelastic modes of the airplane.

With regard to test and analytical techniques, one convenient way to express response characteristics is in terms of frequency response. The longitudinal frequency response may be evaluated directly from flight by measuring the response quantities resulting from sinusoidal elevator motions of various frequencies. However, a considerable saving in flight time is realized if, instead, the airplane is excited by a pulse-type elevator motion and the measured transient time histories are transformed to frequency-response form by the Fourier integral, a technique described in references 1, 2, and 3. In the case of the test airplane, preliminary calculations indicated that pilot-applied pulses would provide adequate excitation over the range of frequencies of interest and, hence, this technique was used. Another application of this method to a relatively flexible airplane is reported in reference 4.

Although these frequency-response data completely define the longitudinal response of the airplane, operational expressions relating the output response to an input disturbance, known as transfer functions, are a more useful form for detailed analysis or for the synthesis of automatic control systems. These transfer functions may be approximated from the measured frequency response by a curve-fitting procedure such as that described in reference 5. Comparable predicted transfer functions may be derived from the equations of motion including rigid body and structural modes.

[redacted]

Simplifications in these transfer functions appeared justified for the range of flight conditions covered in this report. Consequently, theoretical transfer functions were derived from the longitudinal stability equations for two degrees of freedom, and first-order effects of flexibility were included by modifying the coefficients of these simplified transfer functions. The coefficients were calculated for both the rigid and flexible airplane for comparison with coefficients evaluated from flight-test data.

Data used in this report were obtained from flight tests conducted at the High-Speed Flight Research Station of the NACA and the analysis and reduction of data were a cooperative effort of HSFRS and Ames Aeronautical Laboratory.

NOTATION

A	amplitude
C_L	lift coefficient
C_m	pitching-moment coefficient
D	differential operator, $\frac{d}{dt}$
I	imaginary part
K_n	normal-acceleration gain
$K_{\dot{\theta}}$	pitching-velocity gain
K_y	radius of gyration about principal lateral axis, mean aerodynamic chords
M	Mach number
R	real part
S	wing area, sq ft
T_n	normal acceleration time constant, sec
$T_{\dot{\theta}}$	pitching velocity time constant, sec
V	velocity, ft/sec
W	weight, lb
b	wing span, ft

[redacted]

c	wing chord, ft
c.g.	center of gravity, percent $\bar{c}$
$\bar{c}$	wing mean aerodynamic chord, $\frac{2}{S}\int_0^{b/2} c^2 dy$
g	acceleration due to gravity, 32.2 ft/sec^2
i	$\sqrt{-1}$
m	mass, slugs
n	normal acceleration, positive downward, gravity units
q	dynamic pressure, lb/sq in.
$x_{(\ )}$	longitudinal distance from center of gravity to subscript quantity, positive when center of gravity is forward of subscript quantity, ft
y	spanwise coordinate perpendicular to plane of symmetry, ft
z	structural deflection, positive downward, in.
α	angle of attack, radians
δ	elevator control deflection, positive downward, radians, except where noted
ϵ	change in streamwise angle of attack due to wing distortion, radians
ζ	damping ratio, dimensionless
η	spanwise coordinate, fraction of wing semispan
θ	pitch angle, radians
ρ	mass density of air, slugs/cu ft
τ	$\frac{m}{\rho SV}$, sec
$\varphi_{\left(\frac{\text{output}}{\text{input}}\right)}$	phase angle of output quantity minus phase angle of input quantity
ω	frequency, radians/sec

[redacted]

ω_n undamped natural frequency, radians/sec

Subscripts

t tail

wt wing tip

α $\frac{\partial}{\partial \alpha}$

$\dot{\alpha}$ $\frac{\partial}{\partial(d\alpha/dt)}$

θ $\frac{\partial}{\partial \theta}$

$\dot{\theta}$ $\frac{\partial}{\partial(d\theta/dt)}$

$\ddot{\theta}$ $\frac{\partial}{\partial(d\dot{\theta}/dt)}$

δ $\frac{\partial}{\partial \delta}$

TEST EQUIPMENT

The test airplane was a Boeing B-47A with General Electric J-47-GE-23 turbojets and with wing vortex generators as shown in figure 1. The airplane was fitted with an external nose boom and an optigraph on the top of the fuselage which recorded the movement of 100-watt target lights located on both wing panels and on the tail (figs. 1 and 2). Elevator angle was measured by six NACA resistance-type control-position indicators located on the left and right elevators at the root, midsemispan, and tip. The outputs were recorded on Weston 12-channel and Consolidated 18-channel oscillographs. The pitching velocity at the center of gravity was measured by a magnetically damped NACA pitch turn meter, the acceleration at the center of gravity and tail by NACA air-damped accelerometers, and the acceleration at the wing tip by Statham linear accelerometers.

The locations of the optigraph targets and wing stations used in the present study are shown on figure 3. This figure also gives information on the distribution of wing weight which is used subsequently in the analysis.

[redacted]

MEASURED FREQUENCY RESPONSE

Test Procedure

The flight-test conditions covered Mach numbers from 0.6 to 0.85 at an altitude of 35,000 feet for a range of center-of-gravity locations from 12 to 30 percent of the mean aerodynamic chord and a gross weight from about 110,000 to 120,000 pounds. Table I lists the flight conditions used in this report.

Before each maneuver, the airplane was trimmed at the desired speed and altitude. Then the pilot[1] applied a quick elevator pulse and held the stick fixed until the transient motion damped out. It was found that the pilot was capable of consistently applying a 4° to 6° elevator pulse of approximately 0.5-second duration and returning (nearly) to the trim condition. All of these pulses produced about 1/4 g acceleration at the center of gravity. During these maneuvers records were taken of elevator angle, pitching velocity at the center of gravity, normal acceleration at the center of gravity, tail, and wing tips, and wing deflections. Typical time histories of the elevator control input and the measured output quantities are shown on figure 4.

The longitudinal moment of inertia was measured by ground oscillation tests in which the airplane was supported on knife edges and a spring.

Reduction of Data

The transient data measured in flight represent the longitudinal dynamic response of the airplane to a particular elevator input, whereas for detailed analysis it is desirable to know the airplane response to an arbitrary input. As shown in references 1, 2, and 3, it is possible to transform the input and output response quantities into frequency-response form. This defines the response of the airplane to sinusoidal elevator motion of various frequencies. Since the response to any arbitrary input may be obtained by applying an inverse transformation to the frequency response, the frequency response defines all of the basic characteristics of the airplane response independently of the particular input, and in itself provides a means for studying the nature of the response and the effect of variables.

Method.- By means of the Fourier integral the transient function of the input or output, f(t), is for zero initial conditions transformed

[1]Acknowledgement is given to Aeronautical Research Pilots Joseph A. Walker and Stanley P. Butchart.

into the frequency function, $g(i\omega)$, as follows:

$$g(i\omega) = \int_0^\infty f(t)\, e^{-i\omega t}\, dt$$

Separating $g(i\omega)$ into real and imaginary parts gives:

$$R[g(i\omega)] = \int_0^\infty f(t) \cos \omega t\, dt$$

$$I[g(i\omega)] = -\int_0^\infty f(t) \sin \omega t\, dt$$

The amplitude and phase angle obtained from the real and imaginary parts are:

$$A = \sqrt{R^2 + I^2}$$

$$\varphi = \tan^{-1} \frac{I}{R}$$

The method used for evaluating the above integrals was similar to the one described in reference 6, in which ordinates of the time history are read at uniform intervals such that the time history is closely approximated by a series of parabolic arcs. (All traces were read at 0.05-second intervals except for the pitching velocity and wing deflection which were read at 0.1-second intervals.) The integrals were determined by multiplying these ordinates by a set of coefficients for each frequency and then summing the products. Since the ordinates of the time history were read only until a steady-state value was reached, which usually differed from zero, an analytical expression was used for the remaining portion of the integral. These operations were calculated on card-programmed IBM digital computing equipment. Corrections were made in the data for the dynamic response of the instruments.

Accuracy.- The accuracy with which the frequency response may be determined is dependent on the relative magnitudes of the transform of the transient quantities and the transform of errors arising from instrument and reading inaccuracies. These errors in the time history were estimated to be of the order of 0.005 inch of film deflection. Therefore, for linear calibration curves, the transform of the errors consists of

the Fourier transform of random errors up to about 0.005 inch over the length of the transient plus a step error of 0.005 inch in the analytical correction at the end of the record. This latter value is by far the largest and for practical purposes may be considered to be a measure of the maximum expected error. The data in this report were considered to be sufficiently accurate if the amplitude of the Fourier transform of a step of 0.005 inch of film deflection was less than 10 percent of the amplitude of the total transform. If the transform of the errors is out of phase with the transform of the transient, then the error in the amplitude will be less than the value above and the phase angle will be in error. However, this phase-angle error will be less than 6° if the amplitude of the error is less than 10 percent of that of the transient. For this reason, accuracy in the amplitude also insures accuracy in the phase angles.

In initial flight tests a number of pilot-applied elevator pulses of varying length were recorded and the amplitudes of their transforms were compared with the above accuracy criterion as shown on figure 5. The error boundary is the amplitude of the transform of a step of 0.6° elevator deflection (which corresponds to 0.005 inch of film deflection multiplied by 10) and represents a boundary of amplitudes below which errors of greater than 10 percent can be expected. The frequency range was selected to include the first two longitudinal aeroelastic modes indicated by ground vibration tests in reference 7, and the natural frequencies of these modes are marked on this figure. It may be seen that the transform of the longer pulse (run A) tends to go to zero near the frequency of the wing first-bending mode and falls below the accuracy boundary at regular intervals thereafter. Hence, the longer pulse does not provide adequate excitation for accurate evaluation of the frequency response at frequencies of the aeroelastic modes. The shorter pulse (run B), on the other hand, provides adequate excitation for frequencies from 1 to 20 radians per second which is the range of interest in this report. Hence, pulses with a time base of about 0.5 second, as in run B, were used to obtain the frequency-response data in this report.

Frequency-response curves evaluated from transient data in which the airplane was excited by pulses of different lengths at the same flight condition are compared on figure 6. Also shown on this figure are boundaries below which errors of greater than 10 percent would be expected. This error boundary represents the value of $|\dot{\theta}/\delta|$ for which the sum of the separate errors of $|\dot{\theta}|$ and $|\delta|$ is equal to 10 percent. It may be seen that the curves agree within 10 percent over the range where the accuracy criterion is satisfied. At frequencies below 1 radian per second, the frequency response obtained by the shorter pulse becomes inaccurate and the curves disagree. Also, at frequencies above 7 radians per second, the frequency response obtained by the longer pulse becomes inaccurate and it may be seen that the values become erratic. Also shown on this figure is a frequency response evaluated from transient data excited by a short pulse on another flight in which conditions were

[redacted]

slightly different. This curve agrees well with the other frequency-response curve obtained with a short pulse over the frequency range of 1 to 20 radians per second, except that it is displaced upward at all frequencies. As will be shown later, this difference may be accounted for by the difference in the time parameter τ for the two flights. Thus, the data of figure 6 show that with the short-pulse excitation, the frequency response can be evaluated with sufficient accuracy over the frequency range of 1 to 20 radians per second.

Since the frequency-response technique is only valid for linear systems, frequency responses are questionable when obtained at flight conditions in which aerodynamic derivatives are believed to be nonlinear. This airplane appears to have a linear response at 0.72 Mach number and 0.48 lift coefficient since the same frequency response was obtained with different degrees of excitation in figure 6. However, a study of wind-tunnel data indicated that for flight conditions above 0.8 Mach number and for lift coefficients above 0.6 at lower Mach numbers the stability derivatives become nonlinear. In view of this factor caution should be exercised in extrapolating the test results obtained at flight conditions close to these boundaries (see table I for flight conditions) to disturbances greater than those used in the flight tests, that is, $\Delta n_{max} = 1/4$ g at the center of gravity.

No corrections were made in the frequency responses for effects of fuel sloshing.

Results and Discussion

Frequency-response curves evaluated by the foregoing method are shown on figures 7 and 8 for the test range of Mach numbers at an altitude of 35,000 feet; quantities measured at the wing tip and tail as well as at the center of gravity are included so that a fairly complete picture of the response of the airplane is presented. The frequency responses are shown for a forward center-of-gravity location in figure 7 and for a rearward one in figure 8. In the following discussion on these frequency-response curves, the various longitudinal modes will be identified by comparing the accelerations at the center of gravity, wing tip, and tail, and wing deflections. Also, the frequencies at which these modes occur will be compared with those obtained by the ground-vibration tests of reference 7.

Short-period mode.- The first and largest peak in the amplitude ratio of all of the frequency-response curves is the short-period longitudinal mode which occurs at frequencies from 1 to 3 radians per second. These values agree approximately with frequencies estimated from wind-tunnel data. The accelerometer responses at wing tip, tail, and center of gravity, which are compared in figure 9, show that the accelerations

at the three locations are essentially in phase, and that the amplitudes are larger at the wing tip and the tail. The acceleration response at these latter stations differs from that at the center of gravity because of the contributions of structural deflections and pitching acceleration, which will now be discussed.

The wing-bending deflection response, as determined from optigraph records, is presented on figure 10. At the short-period frequency, all deflections are similarly phased and increase in amplitude toward the wing tip, representing a type of deflection similar to the wing first-bending mode. Since for sinusoidal motion acceleration is equal to minus the frequency squared times the displacement, the contribution of the wing deflection to the amplitude ratio of the acceleration at the wing tip is of the order of -1 g per radian. By the same argument, the contribution of tail deflection to the amplitude ratio of the acceleration at the tail was also found to be small. Hence, the contribution of deflections to accelerations at the wing tip and tail are small for frequencies in the neighborhood of the short-period mode.

The contribution of pitching acceleration to the acceleration amplitude at the wing tip and tail may be simply calculated by multiplying the amplitude of the pitching acceleration ($\dot{\theta}\omega$) by the distance to the center of gravity (fig. 2). This is permissible because the phase angles of the acceleration response at the center of gravity and the pitching acceleration response (phase angle of $\ddot{\theta}/\delta$ equals phase angle of $\dot{\theta}/\delta$ plus 90°) are similar at the frequency of 2 radians per second. The increment in acceleration response at the wing tip and tail, then, is about 3 and 5.5 g's per radian, respectively, which agrees with the added increments in the acceleration peak shown on figure 9. Hence, the increase in the acceleration amplitude at the wing and tail is primarily caused by the airplane pitching acceleration.

Comparison of the phase angles on figure 10 with those on figure 9 shows that the wing deflections are in phase with the accelerations and, therefore, the wing tips deflect in proportion to and in the same direction as the airplane accelerates (sketch (a)). This sketch illustrates

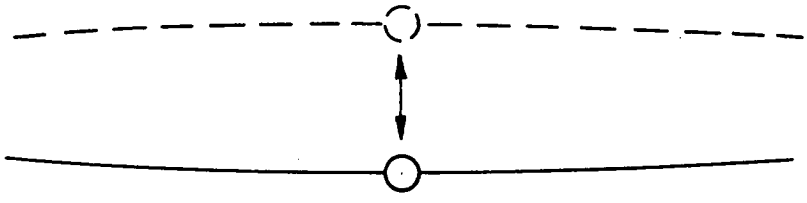

Sketch (a).- Short-period mode.

the relationship of the wing bending to the airplane center-of-gravity motion. Actually, as shown in the discussion of pitching acceleration, the wing tips travel farther in space than the center of gravity because of the pitching motion of the airplane.

[redacted]

Wing first-bending mode.- The next peak in the frequency response, as seen on figures 7, 8, 9, and 10, occurs at frequencies of from 8 to 9 radians per second, slightly higher than the wing first-bending frequency (6.9 radians per second) in ground-vibration tests. Calculations indicate that the frequency of this mode is higher in flight than on the ground because of the additional spring force contributed by aerodynamic forces and the increased freedom of the body in pitch and translation. As seen on figures 7(a) through (c) and 8(a) through (c), the response peaks for locations on the fuselage are small for this mode as compared to those of the short-period mode, but at the wing tip (figs. 7(d) and 8(d)) a very high peak occurs. Referring to figure 9, it is noted that the wing-tip acceleration undergoes a 180° phase shift at this peak. Also, according to figure 10, the amplitudes of the wing deflections increase toward the wing tip and are in phase with each other and 180° out of phase with the wing-tip acceleration which establishes this as the wing first-bending mode. The deflections are also in phase with the acceleration at the center of gravity, as was the case for the short-period mode. The main characteristic which distinguishes this mode from the short-period mode is that the wing deflections are the largest factor in the accelerations at the wing tips (sketch (b)), while in the short-period mode the body translation is the largest factor.

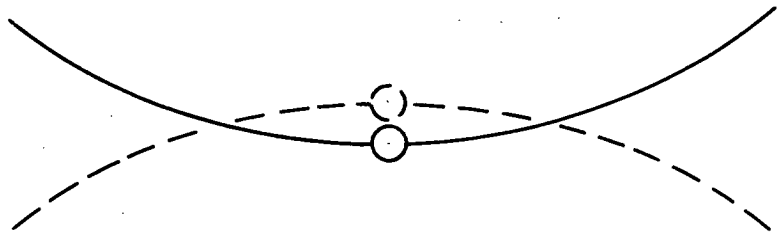

Sketch (b).- Wing first-bending mode.

Other modes.- Several small peaks appear at frequencies from 14 to 16 radians per second, but these are not well defined because the frequency response is in a region of low accuracy. These peaks are most prominent on the wing-tip acceleration responses (figs. 7(d) and 8(d)). The wing-deflection response on figure 10 indicates an upward trend in the mid-semispan-deflection amplitude ratio as compared to that of the wing tip. This would indicate a mode of the wing second-bending type involving body translation and pitch. Some calculations were made on the modes of vibration of the B-47 with body translation and pitch included; these indicated a mode of the type shown in sketch (c) at 16.7

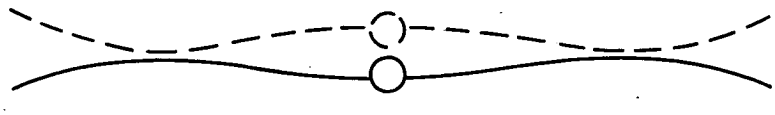

Sketch (c).- Wing second-bending mode coupled with body translation and pitch

[redacted]

radians per second. This agrees qualitatively with the acceleration frequency responses (figs. 7(b), (d) and 8(b), (d)), which show that the accelerations of the wing tip and the center of gravity tend to become more closely phased when the mode becomes prominent at the high Mach numbers. Another possible mode of vibration in this frequency range involves bending of the inboard nacelle supporting structure which, as indicated by ground-vibration tests in reference 7, excites considerable wing motion at 16.4 radians per second. This mode is probably closely coupled with the mode mentioned above, which would explain the appearance of the two closely spaced peaks in this frequency region.

Effect of Mach number and dynamic pressure.- Since Mach number and dynamic-pressure effects cannot be separated when, as in the present case, data are available for only one altitude, they will be considered together with Mach number arbitrarily selected as the independent variable. From figures 7 and 8 it may be seen that there is a gradual increase in the amplitude of the short-period mode peak for the response quantities up to about a Mach number of 0.81, after which the trend reverses, probably because of critical Mach number effects. The general level of the response quantities also follows this trend at the higher frequencies, although the acceleration at the wing tip seems to be relatively insensitive to Mach number changes. At these higher Mach numbers the frequency response is somewhat dependent on the magnitude of the elevator pulse input because of a nonlinear effect mentioned previously.

The frequency of the amplitude peak of the short-period mode also increases up to a Mach number of 0.81 above which it decreases. The frequencies of the peaks of the higher modes are relatively constant over this range of Mach numbers and dynamic pressures, although the same trend may be noted.

Effect of center-of-gravity location.- From figure 11(a) it is seen that the effect of moving the center of gravity from 12.6 to 29.7 has little effect on the frequency response of pitching velocity, although the peaks of the short-period mode occur at lower frequencies as the center of gravity is moved back. The effect of center-of-gravity movement is more apparent on the acceleration response (fig. 11(b)), which shows a definite trend of the short-period mode to higher peaks and lower frequencies as the center of gravity is moved back.

For the rearward center-of-gravity location there are from 3,000 to 4,000 pounds of additional fuel in the aft main tank (fig. 2) as compared with the forward center-of-gravity location. However, there appears to be no significant change in the high-frequency portion (5 to 15 radians per second) of these responses. This might be expected, since the fuselage vertical-bending mode occurs at a much higher frequency (29 radians per second).

[redacted]

EXPERIMENTAL AND PREDICTED TRANSFER FUNCTIONS

Although frequency-response plots completely defined the response characteristics over the frequency range of interest, analytical expressions for the response are more useful in detailed analyses or in the syntheses of automatic control systems. Such analytical expressions, often called transfer functions, may be evaluated either from the experimental frequency-response plots or from the predicted equations of motion of the airplane. In order to show the relationship between the transfer function and the frequency response more clearly, the predicted transfer functions will be derived first. Then the method for evaluating experimental transfer functions will be explained and, finally, the results of the experimental and prediction methods will be compared.

Predicted Transfer Functions

Equations of motion.- To define completely the airplane dynamic system, the equations of motion must include all of the degrees of freedom, but for practical purposes the degrees of freedom are usually kept to a minimum by including only the most significant airplane modes. In the present analysis, only the short-period mode is considered since it was previously shown that the effects of other modes on the responses of principal interest, those involving motions of the fuselage, were small for the test altitude and range of Mach numbers. However, for response quantities near the wing tip where at frequencies near and above the wing first-bending mode frequency the response is large, these equations are, of course, not adequate.

The equations for longitudinal motion, where changes in forward velocity are neglected, were used, with pitching-acceleration ($\ddot{\theta}$) terms added to account for the distortion of the airplane due to pitching-acceleration inertial loads. These equations in operator form are:

$$\left[C_{L_\alpha} + \left(C_{L_{\dot{\alpha}}} + 2\tau\right)D\right]\alpha + \left[\left(C_{L_{\dot{\theta}}} - 2\tau\right)D + C_{L_{\ddot{\theta}}} D^2\right]\theta + C_{L_\delta}\delta = 0 \qquad (1)$$

$$\left(C_{m_\alpha} + C_{m_{\dot{\alpha}}} D\right)\alpha + \left[C_{m_{\dot{\theta}}} D + \left(C_{m_{\ddot{\theta}}} - \frac{4\tau K_y^2 \bar{c}}{2V}\right) D^2\right]\theta + C_{m_\delta}\delta = 0 \qquad (2)$$

In order to account for the first-order effects of flexibility in the preceding equations, the structural deformation associated with a coefficient of the variables α or θ and their derivatives was assumed

to be in phase with the variable, that is, the damping and inertial forces due to structural motion were neglected.

Estimation of stability derivatives.- Stability derivatives were derived by available theory with the exception of the elevator-effectiveness derivatives, which were modified to include additional Mach number effects indicated by wind-tunnel tests. The general methods applied were those of reference 8 to determine airloads and those of reference 9 to account for flexibility effects. Mach number effects were included by the Prandtl-Glauert rule as used in reference 8, which was indicated by wind-tunnel tests to be not greatly in error up to a Mach number of 0.75.

In applying the general methods mentioned above, several modifications were made to facilitate use of structural test data. The structural stiffness of the wing was expressed in the form of influence coefficients for the front- and rear-spar chordwise locations which are compatible with the measured influence coefficients and with the spanwise stations used in determining the span loading in reference 8. These wing influence coefficients were obtained from load deflection data presented in reference 10. The weight distribution shown on figure 3 was separated into equivalent weights as indicated and used with the influence coefficients for determining the wing distortion from inertial loadings. Fuselage influence coefficients were obtained from the Boeing Airplane Company, the airplane manufacturer. Table II lists all the influence coefficients, and Appendix A explains how they were used in conjunction with aerodynamic influence coefficients to calculate the lift, moment, and deflection of the flexible wing and tail due to any initial angle-of-attack distribution. The stability derivatives were calculated by determining the initial angle-of-attack distribution due to rigid-body motions or to distortion from inertial loads caused by rigid-body accelerations, and then calculating the resulting lift and moment coefficients by the method in Appendix A. The derivatives and the related factors which were taken into account are summarized in Appendix B.

The values of the calculated derivatives are given in table III, which lists separately the aerodynamic and inertial contributions. Some of the more important derivatives are compared on figure 12 with values calculated for the rigid airplane. The Mach number effects are reflected by the rigid-airplane derivatives. The flexible-airplane derivatives include both Mach number and flexibility effects and show that flexibility tends to have the opposite effect of Mach number. Of all the derivatives the largest variation occurs in C_{m_α}, but, in general, aeroelastic effects are not exceptionally large because the range of dynamic pressures in these tests is not large.

Evaluation of theoretical transfer functions.- From equations (1) and (2), the following transfer function for pitching velocity may be obtained:

$$\frac{\dot{\theta}}{\delta} = \frac{K_{\dot{\theta}}(1 + T_{\dot{\theta}}D)}{1 + \frac{2\zeta}{\omega_n} D + \frac{1}{\omega_n^2} D^2} \tag{3}$$

and, from the relation $n = -\frac{V}{g}(\dot{\theta} - \dot{\alpha})$

$$\frac{n}{\delta} = \frac{K_n(1 + T_{n_1}D + T_{n_2}D^2)}{1 + \frac{2\zeta}{\omega_n} D + \frac{1}{\omega_n^2} D^2} \tag{4}$$

The acceleration responses at the wing tip and tail are obtained by adding the contributions of acceleration at the center of gravity, the pitching acceleration, and the structural deflection, so that

$$\frac{n_{wt}}{\delta} = \frac{n}{\delta} + \frac{x_{wt}}{g} D\left(\frac{\dot{\theta}}{\delta}\right) + \frac{1}{12g} D^2\left(\frac{z_{wt}}{\delta}\right) \tag{5}$$

and

$$\frac{n_t}{\delta} = \frac{n}{\delta} + \frac{x_t}{g} D\left(\frac{\dot{\theta}}{\delta}\right) + \frac{1}{12g} D^2\left(\frac{z_t}{\delta}\right) \tag{6}$$

where

$$\frac{z}{\delta} = \frac{z}{\alpha}\frac{\alpha}{\delta} + \frac{z}{n}\frac{n}{\delta} + \frac{z}{\dot{\theta}}\frac{\dot{\theta}}{\delta} + \frac{z}{\ddot{\theta}}\frac{\ddot{\theta}}{\delta} \tag{7}$$

$$\omega_n = \left[\frac{-C_{L_\alpha} C_{m_{\dot{\theta}}} + C_{m_\alpha}(C_{L_{\dot{\theta}}} - 2\tau)}{C_{L_{\ddot{\theta}}} C_{m_{\dot{\alpha}}} + \left(\frac{4\tau K_y^2 \bar{c}}{2V} - C_{m_{\ddot{\theta}}}\right)\left(C_{L_{\dot{\alpha}}} + 2\tau\right)}\right]^{1/2} \tag{8}$$

[redacted]

$$\zeta = \frac{\omega_n}{2}\left[\frac{-C_{m_{\dot{\theta}}}\left(C_{L_{\dot{\alpha}}} + 2\tau\right) + C_{L_\alpha}\left(\frac{4\tau K_y{}^2\bar{c}}{2V} - C_{m_{\ddot{\theta}}}\right) + C_{m_{\dot{\alpha}}}\left(C_{L_{\dot{\theta}}} - 2\tau\right) + C_{L_{\ddot{\theta}}}\, C_{m_\alpha}}{-C_{L_\alpha}\, C_{m_{\dot{\theta}}} + C_{m_\alpha}\left(C_{L_{\dot{\theta}}} - 2\tau\right)}\right] \tag{9}$$

$$K_{\dot{\theta}} = \frac{-C_{L_\delta}\, C_{m_\alpha} + C_{L_\alpha}\, C_{m_\delta}}{-C_{L_\alpha}\, C_{m_{\dot{\theta}}} + C_{m_\alpha}\left(C_{L_{\dot{\theta}}} - 2\tau\right)} \tag{10}$$

$$T_{\dot{\theta}} = \frac{-C_{L_\delta}\, C_{m_{\dot{\alpha}}} + C_{m_\delta}\left(C_{L_{\dot{\alpha}}} + 2\tau\right)}{-C_{L_\delta}\, C_{m_\alpha} + C_{L_\alpha}\, C_{m_\delta}} \tag{11}$$

$$K_n = -\frac{V}{g} K_{\dot{\theta}} \tag{12}$$

$$T_{n_1} = \frac{-C_{L_\delta}\left(C_{m_{\dot{\alpha}}} + C_{m_{\dot{\theta}}}\right) + C_{m_\delta}\left(C_{L_{\dot{\alpha}}} + C_{L_{\dot{\theta}}}\right)}{-C_{L_\delta}\, C_{m_\alpha} + C_{L_\alpha}\, C_{m_\delta}} \tag{13}$$

$$T_{n_2} = \frac{C_{L_{\ddot{\theta}}}\, C_{m_\delta} + C_{L_\delta}\left(\frac{4\tau K_y{}^2\bar{c}}{2V} - C_{m_{\ddot{\theta}}}\right)}{-C_{L_\delta}\, C_{m_\alpha} + C_{L_\alpha}\, C_{m_\delta}} \tag{14}$$

Since the transfer-function coefficients are complex combinations of the stability derivatives and mass parameters, certain terms have been grouped together so that the coefficients are analogous to the familiar equations for rigid airplanes. The derivatives $C_{L_{\dot{\theta}}}$ and $C_{L_{\dot{\alpha}}}$ in the terms $C_{L_{\dot{\theta}}} - 2\tau$ and $C_{L_{\dot{\alpha}}} + 2\tau$ represent primarily the change in effective mass of the airplane resulting from lift due to structural distortions. As seen in table III, the aerodynamic contributions to these derivatives are relatively small. The derivative $C_{m_{\ddot{\theta}}}$ in the term $(4\tau K_y{}^2\bar{c}/2V) - C_{m_{\ddot{\theta}}}$

represents the change in effective moment of inertia due to pitching moments arising from structural distortions induced by rotational inertial loads.

Using the stability derivatives given in table III and figure 12, the transfer-function coefficients were calculated for both the flexible and rigid airplane and are shown on figure 13. The coefficient T_{n_1} is not shown because its value is insignificant.

Effect of flexibility on transfer-function coefficients.- The transfer-function coefficients for the rigid and flexible airplane will now be compared to show for the present tests the significance of additional terms included to account for flexibility.

The over-all effect of flexibility on ω_n as shown on figure 13 is to reduce the natural frequency by a maximum of about 10 percent. This is principally caused by the reduction in C_{m_α} due to flexibility of the fuselage. This C_{m_α} effect is partially compensated by a significant increase in the $-C_{L_\alpha}C_{m_{\dot{\theta}}}$ term, which provides an effective spring force resulting from the pitching moments arising principally from wing deflection due to normal acceleration. The term $C_{m_{\ddot{\theta}}}$ in the denominator tends to increase the frequency by about 5 percent.

The effect of flexibility on damping ratio, ζ, is small as shown on figure 13. The damping forces are reduced by flexibility, but the spring and inertial forces are also reduced to such an extent that the over-all effect of flexibility on damping ratio is insignificant.

The pitching-velocity gain, $K_{\dot{\theta}}$, of the flexible airplane is somewhat higher than that of the rigid airplane (fig. 13). This change is principally due to the reduction in magnitude of C_{m_α} in the denominator which also is in part compensated by the increase in $C_{m_{\dot{\theta}}}$. Because of this large contribution of $C_{m_{\dot{\theta}}}$ for the flexible airplane, increments in gain for a 10-percent increase in τ given on figure 13 show that the flexible airplane has about a 15-percent smaller change in gain due to changes in gross weight and altitude.

Flexibility has little effect on $T_{\dot{\theta}}$ as shown on figure 13. Although the reduction in C_{L_α} due to flexibility tends to increase $T_{\dot{\theta}}$, this is compensated for the most part by the effective reduction in mass in the numerator term.

The discussion of $K_{\dot{\theta}}$ applies to K_n, since these factors are related by a simple constant.

The term T_{n_1} is exceptionally small and is not significant over the range of frequencies considered in this report.

[redacted]

Flexibility tends to increase T_{n_2} (fig. 13). Although this term is small, it does have a noticeable effect at frequencies greater than that of the short-period mode.

Effect of approximate equations on transfer-function coefficients.- Approximate equations are often used for calculating the transfer-function coefficients. These equations, which are obtained by simplifying equations 8, 9, 10, and 11, are as follows:

$$\omega_n = \left(\frac{-C_{m_\alpha}}{4\tau K_y^2 \frac{\bar{c}}{2V}} \right)^{1/2} \tag{15}$$

$$\zeta = \left(\frac{-\rho S \bar{c}}{32 m K_y^2 C_{m_\alpha}} \right)^{1/2} \left(2K_y^2 C_{L_\alpha} - C_{m_{\dot{\theta}\frac{\bar{c}}{2V}}} - C_{m_{\dot{\alpha}\frac{\bar{c}}{2V}}} \right) \tag{16}$$

$$K_{\dot{\theta}} = \frac{-C_{L_\alpha} C_{m_\delta}}{2\tau C_{m_\alpha}} \tag{17}$$

$$T_{\dot{\theta}} = \frac{2\tau}{C_{L_\alpha}} \tag{18}$$

Transfer-function coefficients for the rigid and flexible cases were calculated using both the complete and the approximate equations and the results are shown on figure 14.

Coefficients evaluated by the approximate equations show reasonably good agreement with those from the complete equations for the rigid airplane, but large discrepancies are apparent in the case of ω_n and $K_{\dot{\theta}}$ for the flexible airplane. This is principally due to the fact that the approximate equations reflect only the large reduction in magnitude of C_{m_α} due to flexibility while in the complete equations, the effect of this reduction in magnitude of C_{m_α} is partially compensated by a substantial increase in the term $-C_{L_\alpha} C_{m_{\dot{\theta}}}$. Hence, it may be seen that $C_{m_{\dot{\theta}}}$ should not be neglected in calculating the frequency and gain of a flexible airplane.

[redacted]

Experimental Transfer Functions

Experimental transfer functions may be evaluated by applying various curve-fitting procedures to the time histories or to the frequency responses. Curve fitting of a time history may be accomplished by a least-squares fitting method such as described in reference 11. Curve fitting of the frequency response, as in the following analysis, may be done by use of a special set of templates described in reference 5. This method may be explained briefly as follows. It can be shown that an expression for frequency response is obtained by replacing the differential operator, D, in the transfer function by the frequency variable, $i\omega$. The resulting complex number can be factored into first- and second-order terms expressed in polar (amplitude and phase angle) form. The method of reference 5 involves fitting the measured frequency response by graphical addition of templates selected from a set of curves which represent a wide range of first- and second-order factors.

Evaluation of transfer-function coefficients.- As shown previously, the accuracy of the frequency response at low frequencies is questionable. For this reason, template fitting of the frequency response was only considered to be valid for frequencies above 1 radian per second. This limitation made it difficult to fit the frequency response by a unique combination of templates for all of the numerator and denominator terms which are involved simultaneously in the frequency-response expression. Because of this, the natural frequency and damping ratio were determined by a least-squares curve-fitting method (similar to that of reference 11) of the pitching-velocity time history over the portion of the record in which rate of change of elevator position could be neglected. The appropriate templates for these values of damping ratio and natural frequency were then fitted to the center-of-gravity acceleration frequency-response curves to obtain the acceleration gain, K_n, and the time constant, T_{n_2}. The gain $K_{\dot{\theta}}$ was then determined from K_n. By use of this value of $K_{\dot{\theta}}$ and the previously determined values of ζ and ω, the pitching-velocity frequency response was fitted to determine $T_{\dot{\theta}}$. A typical template fit is shown on figures 7(a) and (b) for the 0.63 Mach number curve.

Transfer-function coefficients evaluated from experimental data for the forward and rearward center-of-gravity locations are plotted on figure 15. These values were corrected to a common altitude and gross weight in accordance with predicted variations, but in general these corrections were small.

Comparison of Experimental and Predicted Transfer Functions

Predicted transfer-function coefficients for the rigid and flexible airplane are also shown on figure 15 for comparison with the experimental

values. The moment of inertia used in the predicted coefficients was determined from ground-oscillation tests for the basic airplane, with corrections made for condition of the fuel tanks. The stability derivatives of table III were employed.

Effect of Mach number.- Referring to figure 15, it may be seen that the experimental values of natural frequency show good agreement with the predicted values for the flexible airplane and fall about 10 percent below those predicted for the rigid airplane. An exception is noted at a Mach number of 0.84 where the measured frequency decreases sharply, probably due to the large decrease in C_{m_α} as the airplane approaches the pitch-up. Also on this figure, it is seen that the scatter in the measured damping-ratio points prohibits definite confirmation of the predicted small variations with Mach number, center-of-gravity location, and flexibility. However, the general level of the values shows good agreement with theory.

On figure 15 good agreement is indicated for the pitching-velocity gain except at Mach numbers of 0.8 and higher, where large unpredicted increases in the measured gain are apparent. This again is probably the result of the sudden decrease in the static margin as the critical Mach number is approached as previously mentioned. On this figure, good agreement also is indicated for the pitching-velocity time constant, $T_{\dot{\theta}}$, although the experimental values tend to fall consistently a small amount below the predicted ones.

Effect of center-of-gravity location.- On figure 16, the variation of natural frequency and damping ratio with center-of-gravity location is shown for several Mach numbers. The measured values of natural frequency show good agreement with the frequencies predicted for the flexible airplane over the test range of center-of-gravity locations. The frequencies predicted for the rigid airplane are consistently higher than those for the flexible airplane, but show about the same variation with center-of-gravity movement as for the flexible airplane. The measured and predicted damping ratios show fairly small changes with center-of-gravity location.

In summary, the longitudinal response of the airplane may be adequately predicted by the theory used herein to account for flexibility up to a Mach number of 0.8. The largest errors occur in the natural frequency if flexibility is not taken into account, but in general all of the transfer-function coefficients show only small changes over the airplane range of dynamic pressures at 35,000 feet.

Since the transfer-function coefficients are relatively insensitive to flexibility effects at these flight conditions, a more sensitive transfer function, the wing-tip deflection response, was calculated from equation (7) in order to provide a more accurate check on the aeroelastic calculations. The method of calculating deflections is shown

in Appendix A. The comparison between experimental and predicted values in frequency-response form is shown in figure 17. It may be seen that the amplitude ratios agree very well and that the phase angles of the experimental response tend to lag the predicted ones 20° to 30° up to frequencies of 5 radians per second. From this, it would appear that the theoretical calculations of the contribution of the wing to the stability derivatives are accurate except for a small phase lag which is probably due to the inertial and damping forces due to wing bending motion which were neglected in the theory.

CONCLUSIONS

The evaluation of the dynamic response of a large flexible airplane to elevator pulses at 35,000 feet over a Mach number range of 0.6 to 0.85 and the comparisons with predicted response have led to the following conclusions:

1. The pulse technique provides dynamic-response data that are sufficiently accurate for evaluation of frequency response from 1 to 20 radians per second, a frequency range which includes the first two aeroelastic modes.

2. Except at conditions where the airplane has a pitch-up tendency, good agreement between predicted and experimental transfer functions is obtained for frequencies near that of the short-period mode, using predictions based on the usual two-degree-of-freedom form of transfer function in which the coefficients were modified to include zero-frequency aeroelastic effects.

3. For frequencies near and above that of the wing first-bending mode, the modified two-degree-of-freedom theory is inadequate. However, the response amplitudes at the center of gravity and tail which are associated with airplane structural modes are small compared to the response amplitude of the short-period mode and could be neglected for this range of flight conditions. On the other hand, the response amplitudes near the wing tip become relatively high at these frequencies and could not be neglected.

4. For the flight-test conditions, the principal effects of airplane flexibility are to decrease the natural frequency and increase the steady maneuvering acceleration per unit elevator deflection, trends which may be attributed principally to fuselage and tail bending and the associated loss in the angle-of-attack moment derivative, C_{m_α}. This C_{m_α} effect would be more significant if it were not compensated partially by the effect of the increase in the rate-of-pitch moment derivative, $C_{m_{\dot{\theta}}}$, due to normal acceleration.

[redacted]

5. The method of employing aerodynamic and structural influence coefficients in aeroelastic calculations which was used in this investigation proved to be advantageous in simplifying spanwise loading calculations and in applying static-test load data.

Ames Aeronautical Laboratory
National Advisory Committee for Aeronautics
Moffett Field, Calif., Aug. 9, 1954

[redacted]

APPENDIX A

A METHOD FOR DETERMINING THE AERODYNAMIC LIFT AND MOMENT OF A FLEXIBLE WING THROUGH USE OF INFLUENCE COEFFICIENTS

The approach used is generally that presented in reference 9. However, for the calculation of wing deformations, the use of structural influence coefficients in conjunction with aerodynamic influence coefficients will be introduced in place of the wing bending and torsional stiffness distributions EI and GJ, and the distributed aerodynamic loadings used in reference 9.

The loading on a flexible wing may be separated into two parts: that of the rigid wing and that produced by the wing deflection. The discussion that follows will be concerned with the determination of the loading produced by a wing deflection corresponding to a given rigid-wing loading. The change in streamwise angle of attack due to wing deformation may be expressed in a power series form as

$$\epsilon(\eta) = \epsilon_0(\eta)q + \epsilon_1(\eta)q^2 + \epsilon_2(\eta)q^3 + \ldots \tag{A1}$$

where

$\epsilon_0(\eta)$ is the angle-of-attack distribution due to rigid-wing loading

$\epsilon_1(\eta)$ is the angle-of-attack distribution due to loading obtained from $\epsilon_0(\eta)$

$\epsilon_2(\eta)$ is the angle-of-attack distribution due to loading obtained from $\epsilon_1(\eta)$

The incremental angle-of-attack distributions $\epsilon_0(\eta)$, $\epsilon_1(\eta)$ may be converted into incremental lifts to form the series

$$\Delta C_L = C_{L_A}\, q + C_{L_B}\, q^2 + C_{L_C}\, q^3 + \ldots$$

As shown in reference 9, this series can be represented very nearly by the equation

$$\Delta C_L = \frac{C_{L_A}\, q}{1 + kq} \tag{A3}$$

[redacted]

where

$$k = -\frac{C_{L_B}}{C_{L_A}} = -\frac{C_{L_C}}{C_{L_B}}, \text{ etc.}^1$$

The total lift coefficient for the flexible wing may be written as

$$C_{L_F} = C_{L_R}\left(1 + \frac{q}{1 + kq}\frac{C_{L_A}}{C_{L_R}}\right) \tag{A4}$$

where C_{L_R} is the lift coefficient for the rigid wing. Similar equations may be written for the aerodynamic moment coefficient.

Thus it remains to determine C_{L_A}/C_{L_R} and k through use of the influence coefficients. The aerodynamic influence coefficients were obtained in the form of the loading coefficient $G_{\nu n}$ at a station n due to a unit angle of attack at station ν, the angle of attack at the other stations being zero. The loading coefficients were obtained by the method of reference 8. By use of this method, aerodynamic influence coefficients at four spanwise stations could be found which, with proper care, were sufficient to provide desired accuracy in determining wing deflections. These coefficients, $G_{\nu n}$, were obtained by assuming a unit angle of attack at one control point, and zero angle of attack at the remaining three, and then solving the set of four simultaneous equations consisting of the $a_{\nu n}$ coefficients obtained from reference 8. For instance, G_{1n} can be calculated from the following simultaneous equations

$$1 = a_{11}G_{11} + a_{12}G_{12} + a_{13}G_{13} + a_{14}G_{14}$$

$$0 = a_{21}G_{11} + a_{22}G_{12} + a_{23}G_{13} + a_{24}G_{14}$$

$$0 = a_{31}G_{11} + a_{32}G_{12} + a_{33}G_{13} + a_{34}G_{14}$$

$$0 = a_{41}G_{11} + a_{42}G_{12} + a_{43}G_{13} + a_{44}G_{14}$$

---

[1]In reference 9, the constant k was determined by the ratios of the incremental deflections

$$k = -\frac{\epsilon_1(\eta)}{\epsilon_0(\eta)} = -\frac{\epsilon_2(\eta)}{\epsilon_1(\eta)}, \text{ etc.}$$

However, for the present method, it will be more convenient to deal directly with the incremental lifts.

where subscripts 1, 2, 3, and 4 refer to the semispan stations $\eta = 0.924$, 0.707, 0.383, and 0. The resulting lift coefficient for each unit angle of attack can then be calculated using the equation

$$C_{L_\nu} = \frac{\pi A}{8}\left(G_{\nu 4} + 1.848G_{\nu 3} + 1.414G_{\nu 2} + 0.765G_{\nu 1}\right) \tag{A5}$$

The experimentally determined structural influence coefficients (ref. 10) were measured in the form of deflections in inches at front and rear spars due to 1,000-pound loads at front and rear spars at a number of spanwise stations. These were cross-plotted to obtain the influence coefficients at the spanwise stations shown in table II. For use with the aerodynamic influence coefficients, these coefficients were further reduced into the form of a change in streamwise angle of attack in radians, due to a 1,000-pound load at the quarter-chord position, S_{mn}.

The influence deflections due to a unit angle of attack at a control station can now be calculated through use of the aerodynamic and structural influence coefficients. In order to calculate the deflections with sufficient accuracy, an integration formula given in reference 8 was used.

$$\int_{-1}^{1} f(\eta)\, d\eta = \frac{\pi}{l+1} \sum_{n=1}^{l} f(\eta_n) \sin \varphi_n$$

where $\varphi_n = \frac{n\pi}{l+1}$ and $f(\eta_n)$ is the value of $f(\eta)$ at $\eta = \cos \frac{n\pi}{l+1}$. For the particular number of control stations used in the present case, and since $f(\eta_4) = 0$, and using only the interval $0 < \eta < 1$, the integration formula becomes

$$\int_{0}^{1} f(\eta)\, d\eta = \sum_{n=1}^{3} f(\eta_n)\, I_n \tag{A6}$$

where

$$I_1 = 0.1502$$

$$I_2 = 0.2776$$

$$I_3 = 0.3628$$

Thus, the angular deflection at station m due to loading due to angle of attack at station ν, with $q = 1$ psi is calculated from the equation

$$(\epsilon_o)_{\nu m} = \frac{b^2(12)^2}{1000} \sum_{n=1}^{3} G_{\nu n} S_{mn} I_n \tag{A7}$$

with

$$m = 1, 2, 3$$

$$\nu = 1, 2, 3, 4$$

The resulting loading due to $(\epsilon_o)_{\nu m}$ is calculated from the equation

$$(G_A)_{\nu n} = \sum_{m=1}^{3} (\epsilon_o)_{\nu m} G_{mn} \tag{A8}$$

from which the lift coefficient may be obtained

$$\left(C_{L_A}\right)_\nu = \frac{\pi A}{8}\left[(G_A)_{\nu 4} + 1.848(G_A)_{\nu 3} + 1.414(G_A)_{\nu 2} + 0.765(G_A)_{\nu 1}\right] \tag{A9}$$

The influence lift coefficient, $\left(C_{L_B}\right)_\nu$, due to deflections due to the loading coefficient $(G_A)_{\nu n}$ can be calculated in a similar manner. The equation for $\left(C_{L_B}\right)_\nu$ is

$$\left(C_{L_B}\right)_\nu = \frac{\pi A}{8}\left[(G_B)_{\nu 4} + 1.848(G_B)_{\nu 3} + 1.414(G_B)_{\nu 2} + 0.765(G_B)_{\nu 1}\right] \tag{A10}$$

Thus, for a given angle-of-attack distribution, α_ν, the lift resulting from the initial angle of attack and from the first and second twist distributions is calculated from the following equations

$$C_{L_R} = \sum_{\nu=1}^{4} C_{L_\nu} \alpha_\nu \tag{A11}$$

$$C_{L_A} = \sum_{\nu=1}^{4} \left(C_{L_A}\right)_{\nu} \alpha_{\nu} \tag{A12}$$

$$C_{L_B} = \sum_{\nu=1}^{4} \left(C_{L_B}\right)_{\nu} \alpha_{\nu} \tag{A13}$$

The total lift for the flexible wing may then be expressed as

$$C_{L_F} = C_{L_R}\left(1 + \frac{q\,\frac{C_{L_A}}{C_{L_R}}}{1 + kq}\right) \tag{A14}$$

where

$$k = -\frac{C_{L_B}}{C_{L_A}}$$

A similar procedure is used to obtain the aerodynamic moment for a flexible wing.

Wing deflections may also be determined by means of wing-deflection influence coefficients in a manner similar to that which was used for determining the change in streamwise angle of attack. The deflection at station m due to the loading due to angle of attack at station ν, with $q = 1$ psi is calculated from the equation

$$(z_o)_{\nu m} = \frac{b^2(12)^2}{1000} \sum_{n=1}^{3} G_{\nu n} Z_{mn} I_n \tag{A15}$$

with

$$m = 1, 2, 3$$

$$\nu = 1, 2, 3, 4$$

where Z_{mn} is the deflection in inches at station m due to a 1,000-pound load at the quarter chord at spanwise station n.

[redacted]

For an arbitrary angle-of-attack distribution, the deflection at station m due to the initial load is

$$(z_o)_m = \sum_{\nu=1}^{4} (z_o)_{\nu m} \alpha_\nu \tag{A16}$$

The total deflection for the flexible wing may be developed in a manner similar to that used for equation (A14). Then

$$z_m = \frac{q}{1 + kq} (z_o)_m \tag{A17}$$

in which the k from equation (A14) may be used with sufficient accuracy.

APPENDIX B

EVALUATION OF STABILITY DERIVATIVES

C_{L_α}

Wing lift-curve slope.- This was determined theoretically from reference 8 and Appendix A using the section lift-curve slope of 5.71 as determined from wind-tunnel data supplied by the Boeing Airplane Company. This derivative should not be confused with the one in reference 12, which includes inertial effects. The present derivative is the one which would be evaluated experimentally in a wind tunnel with a flexible model.

Tail lift-curve slope.- This was determined in a manner similar to that of the wing, except that fuselage bending was included in the flexibility of the tail. It was found that the principal reduction in the tail lift-curve slope was caused by fuselage bending. Other factors included were the rate of change of downwash (ref. 13) and a tail efficiency factor of 0.95.

Body and nacelles lift-curve slope.- This was determined from wind-tunnel data supplied by the Boeing Airplane Company.

$C_{L_{\dot{\alpha}}}$

Lag in wing downwash.- Only the tail contribution was considered and was determined in a manner similar to that described in reference 14, including aeroelastic effects determined by the method of Appendix A. Although this term has small effect from the standpoint of lift, it is important in the calculation of $C_{m_{\dot{\alpha}}}$.

Normal acceleration.- Since normal acceleration is related to $\dot{\alpha}$ in the equation $n = -\frac{V}{g}(\dot{\theta} - \dot{\alpha})$, effects of structural deflections due to normal acceleration were included in derivatives in $\dot{\alpha}$ and $\dot{\theta}$ by the method of Appendix A. The principal contribution to this derivative is from the lift of the wing. Contribution of the tail varies according to the amount of fuel in the rear main tank and is from 10 to 20 percent of the total.

$C_{L_{\dot{\theta}}}$

Lift arising from angle-of-attack distribution due to pitching velocity (primarily a tail contribution) was determined using the method of Appendix A.

Normal acceleration.- Same as normal acceleration part of $C_{L_{\dot{\alpha}}}$, but of opposite sign.

$C_{L_{\ddot{\theta}}}$

Lift resulting from angle-of-attack distribution caused by structural distortion due to rotational inertial loads was determined by the method of Appendix A. Primarily a wing contribution, but the total effect is small.

$C_{L_{\delta}}$

Rigid-airplane value was obtained from low-speed wind-tunnel data supplied by the Boeing Airplane Company and was assumed to be constant with Mach number. This is justified because the theoretical increase according to the Prandtl-Glauert rule is usually compensated by the pressure losses at the elevator hinge point (ref. 15). Aeroelastic effects of lift and moment on body bending and of lift on stabilizer distortion were included. Stabilizer distortion due to elevator pitching moment and elevator distortion were neglected.

$C_{m_{\alpha}}$

This derivative was determined by multiplying the preceding $C_{L_{\alpha}}$ derivatives by the distance in mean aerodynamic chord lengths from their theoretical centers of pressure to the center of gravity. The value of $C_{m_{\alpha}}$ for body and nacelles was obtained by subtracting the theoretical $C_{m_{\alpha}}$ for wing alone from wind-tunnel values of $C_{m_{\alpha}}$ for wing, body, and nacelles. It should be noted that this also includes the change in $C_{m_{\alpha}}$ due to the difference between theoretical and experimental $C_{m_{\alpha}}$ of wing alone, a difference which is principally due to a somewhat higher loading near the root for the experimental than for the theoretical case. Since this additional loading occurs near the wing root, it does not affect the aeroelastic calculations and, hence, is appropriately

[redacted]

added to C_{m_α} in the form of a correction for body pitching moment.

$$C_{m_{\dot{\alpha}}},\ C_{m_{\dot{\theta}}},\ C_{m_{\ddot{\theta}}},\ C_{m_\delta}$$

These moment derivatives were determined by multiplying the corresponding lift derivatives by their moment arms in a manner similar to that described for C_{m_α}.

REFERENCES

1. Seamans, R. C., Jr., Blasingame, B. P., and Clementson, G. C.: The Pulse Method for the Determination of Aircraft Dynamic Performance. Jour. Aero. Sci., vol. 17, no. 1, Jan. 1950, pp. 22-38.

2. Breaux, G. P., and Zeiller, E. L.: Dynamic Response Program on the B-36 Airplane. Part III - Presentation and Theoretical Considerations of the Transient Analysis Method Employed for Obtaining Frequency Response Functions from Flight Data. Consolidated Vultee Aircraft Corp., Rep. FZA-36-195, Feb. 14, 1952.

3. Triplett, William C., and Smith, G. Allan: Longitudinal Frequency-Response Characteristics of a 35° Swept-Wing Airplane as Determined From Flight Measurements, Including a Method for the Evaluation of Transfer Functions. NACA RM A51G27, 1951.

4. Marx, H. F., Clemen, A. T., and Zant, W. L.: Frequency Response Characteristics of the B-36D Airplane. Part I - Lateral Response at 40,000 Feet. Consolidated Vultee Aircraft Corp., Rep. FZA-36-256, Jan. 24, 1952.

5. Lees, Sidney: Graphical Aids for the Graphical Representation of Functions of the Imaginary Argument. M.I.T., Inst. Lab. Eng. Memo. E-25, 1951.

6. Schumacher, Lloyd E.: Methods for Analyzing Transient Flight Data to Obtain Aircraft Frequency Response. AF, Air Materiel Command, Wright-Patterson AFB (Flight Test Div. Memo. Rep.) Ser. MCRFT-2268, Jan. 1950.

7. Flutter Inspection of Boeing XB-47 Airplane. AF, Air Materiel Command, Wright-Patterson AFB (E.D.M.R.) Ser. MCREXAS-4262-36-29, 1948.

8. DeYoung, John, and Harper, Charles W.: Theoretical Symmetric Span Loading at Subsonic Speeds for Wings Having Arbitrary Plan Form. NACA Rep. 921, 1948.

9. Skoog, Richard B., and Brown, Harvey H.: A Method for the Determination of the Spanwise Load Distribution of a Flexible Swept Wing at Subsonic Speeds. NACA TN 2222, 1951. (Supersedes NACA RM A50G31)

10. Mayo, Alton P., and Ward, John F.: Experimental Influence Coefficients for the Deflection of the Wing of a Full-Scale, Swept-wing Bomber. NACA RM L53L23, 1954.

[redacted]

11. Shinbrot, Marvin: A Least Squares Curve Fitting Method With Applications to the Calculation of Stability Coefficients From Transient-Response Data. NACA TN 2341, 1951.

12. Skoog, Richard B.: An Analysis of the Effects of Aeroelasticity on Static Longitudinal Stability and Control of a Swept-Back-Wing Airplane. NACA RM A51C19, 1951.

13. Diederich, Franklin W.: Charts and Tables for Use in Calculations of Downwash of Wings of Arbitrary Plan Form. NACA TN 2353, 1951.

14. Perkins, Courtland D., and Hage, Robert E.: Airplane Performance Stability and Control. John Wiley & Sons, Inc., 1949.

15. Tinling, Bruce E., and Dickson, Jerald K.: Tests of a Model Horizontal Tail of Aspect Ratio 4.5 in the Ames 12-Foot Pressure Wind Tunnel. I - Quarter-Chord Line Swept Back 35°. NACA RM A9G13, 1949.

[redacted]

TABLE I.- FLIGHT-TEST CONDITIONS

Flight number	Run number	Altitude	Mach no.	C_L	W	c.g.	K_y^2	τ
2	16	36,170	0.68	0.56	121,400	20.9	2.4	5.8
	18a	35,500	.72	.48	120,900	20.9	2.4	5.2
	18b	35,500	.72	.48	120,900	20.9	2.4	5.2
	20	36,260	.78	.41	120,000	21.1	2.4	4.9
	21	34,860	.82	.38	119,800	21.1	2.4	4.4
	22	34,860	.84	.33	119,300	21.1	2.4	4.3
	23	34,100	.85	.28	118,200	21.8	2.4	4.1
	25	32,230	.63	.49	113,600	21.0	2.5	4.9
	26	35,950	.62	.61	113,200	21.0	2.5	5.8
3	15	35,070	.63	.63	116,100	12.7	2.5	5.6
	16	35,090	.66	.55	115,900	12.6	2.5	5.3
	17	35,360	.71	.48	115,900	12.6	2.5	5.0
	18	35,060	.74	.45	115,900	12.5	2.5	4.7
	19	34,980	.77	.38	115,900	12.4	2.5	4.5
	20	34,960	.81	.37	115,700	12.5	2.5	4.4
	21	35,150	.82	.36	115,600	12.5	2.5	4.3
	22	35,600	.84	.36	115,500	12.3	2.5	4.3
5	1	35,840	.79	.40	119,100	24.9	2.4	4.8
	3	34,170	.73	.43	118,200	24.8	2.4	4.6
	4	34,070	.69	.48	117,800	24.6	2.4	4.9
	5	34,220	.65	.54	117,000	24.6	2.4	5.3
	6	35,100	.60	.66	116,600	24.6	2.4	5.9
	15	35,950	.72	.45	111,100	21.6	2.4	4.9
9	19	34,860	.73	.43	116,200	29.7	2.4	4.8
	22	34,590	.60	.60	115,300	29.5	2.4	5.8
	20	34,780	.70	.43	116,200	29.7	2.4	5.0
	16	34,960	.81	.37	116,800	29.8	2.4	4.4

TABLE II.- STRUCTURAL INFLUENCE COEFFICIENTS

Wing									
		1000-pound load at station[1]							
		3F[1]	3R[1]	2F	2R	1F	1R	5F	5R
Inches deflection at station[1]	3F	0.0659	0.0580	0.1765	0.1663	0.2447	0.2307	0.2033	0.1936
	3R	.0705	.0931	.2116	.2398	.3057	.3339	.2486	.2784
	2F	.1769	.2052	.7419	.7795	1.2134	1.2490	.9285	.9590
	2R	.1804	.2318	.7881	.9005	1.3309	1.4300	.9995	1.1070
	1F	.2302	.2730	1.1943	1.2934	2.3486	2.3840	1.6374	1.7184
	1R	.2330	.2940	1.2430	1.4057	2.4598	2.5920	1.7086	1.8677

Fuselage	
Load	Change in stabilizer angle
1g Normal acceleration	-0.45°
1 Radian/sec^2 pitching acceleration.	-0.521° (c.g. = 17 percent), -0.506° (c.g. = 25 percent)
1,000-pound tail load (down)	+3.42°
1,000 inch-pounds moment applied at stabilizer.	0.000207°

[1]Station locations are shown on figure 3. F denotes front spar location. R denotes rear spar location.

[redacted]

TABLE III.- PREDICTED LONGITUDINAL STABILITY DERIVATIVES FOR THE FLEXIBLE AIRPLANE AT AN ALTITUDE OF 35,000 FEET; W = 100,000 POUNDS

Quantity	c.g.	Mach number				
		0	0.5	0.6	0.7	0.8
C_{L_α}	---	5.27	5.31	5.36	5.45	5.6
Aerodynamic $C_{L_{\dot\alpha}}$	---	7.1/V	.015	.013	.011	.010
Aerodynamic $C_{L_{\dot\theta}}$	0.12 .25	36/V 27.2/V	.069 .050	.056 .040	.046 .032	.038 .025
Inertial $C_{L_{\dot\theta}}$ and $-C_{L_{\dot\alpha}}$	.12 .25	$.026\frac{V}{g}$ $.027\frac{V}{g}$	.348 .373	.401 .431	.444 .480	.473 .512
$C_{L_{\ddot\theta}}$	.12 .25	-.034 -.030	-.031 -.027	-.030 -.026	-.029 -.025	-.028 -.024
C_{m_α}	.12 .25	-1.68 -1.01	-1.81 -1.14	-1.82 -1.15	-1.82 -1.11	-1.81 -1.08
Aerodynamic $C_{m_{\dot\alpha}}$	.12 .25	-27/V -26/V	-.053 -.050	-.047 -.045	-.040 -.039	-.036 -.035
Aerodynamic $C_{m_{\dot\theta}}$	.12 .25	-146/V -138/V	-.302 -.288	-.256 -.244	-.224 -.213	-.204 -.192
Inertial $-C_{m_{\dot\theta}}$ and $C_{m_{\dot\alpha}}$	.12 .25	$.024\frac{V}{g}$ $.024\frac{V}{g}$	.337 .338	.398 .400	.451 .457	.489 .499
$C_{m_{\ddot\theta}}$	.12 .25	.031 .030	.030 .029	.029 .028	.028 .027	.028 .027
C_{L_δ}	---	.327	.312	.306	.299	.292
C_{m_δ}	.12 .25	-1.21 -1.17	-1.16 -1.12	-1.14 -1.09	-1.11 -1.07	-1.08 -1.05
τ	---	2940/V	6.05	5.03	4.31	3.77

NACA

[redacted]

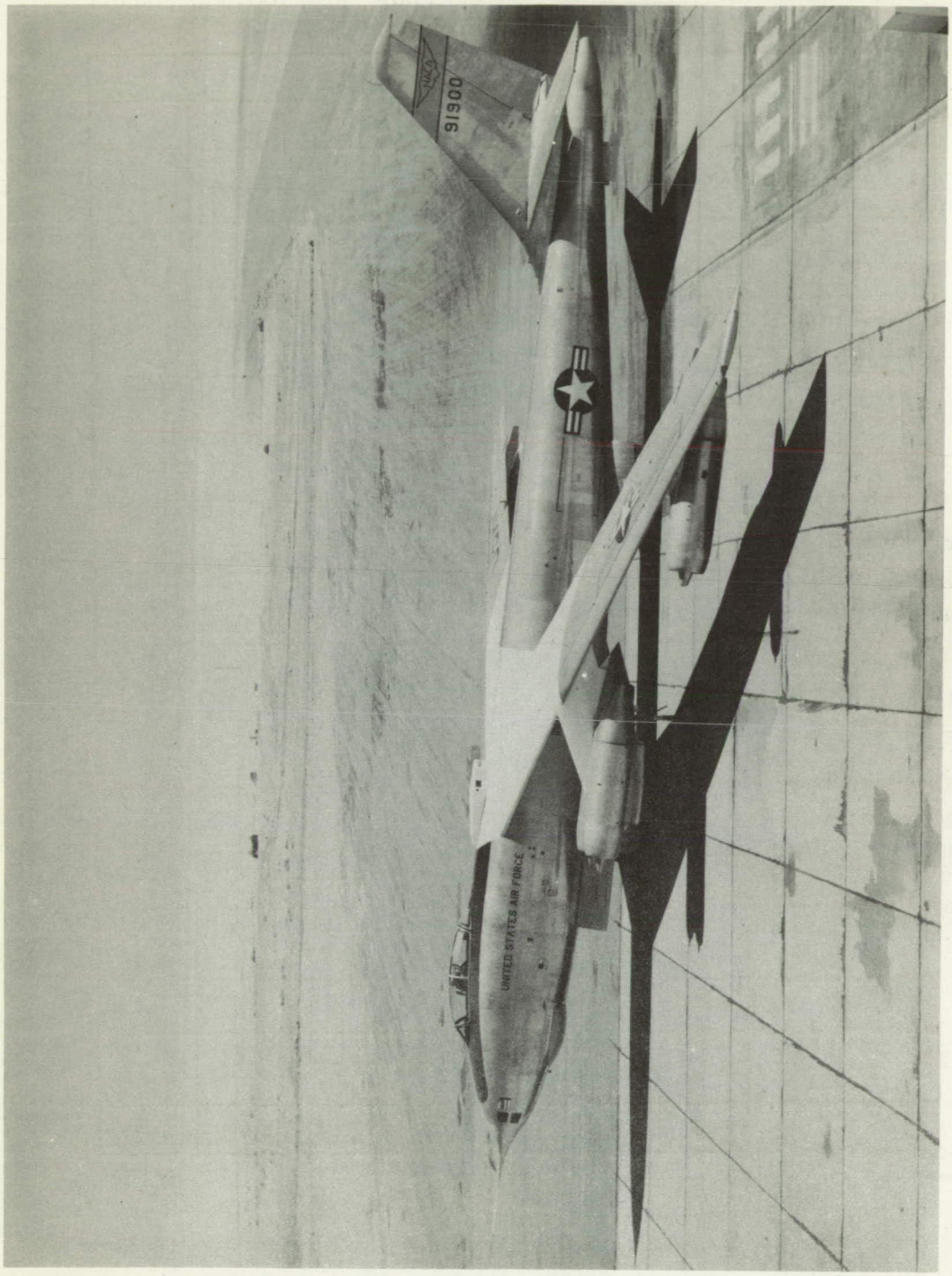

A-19582

Figure 1.- Photograph of the test airplane.

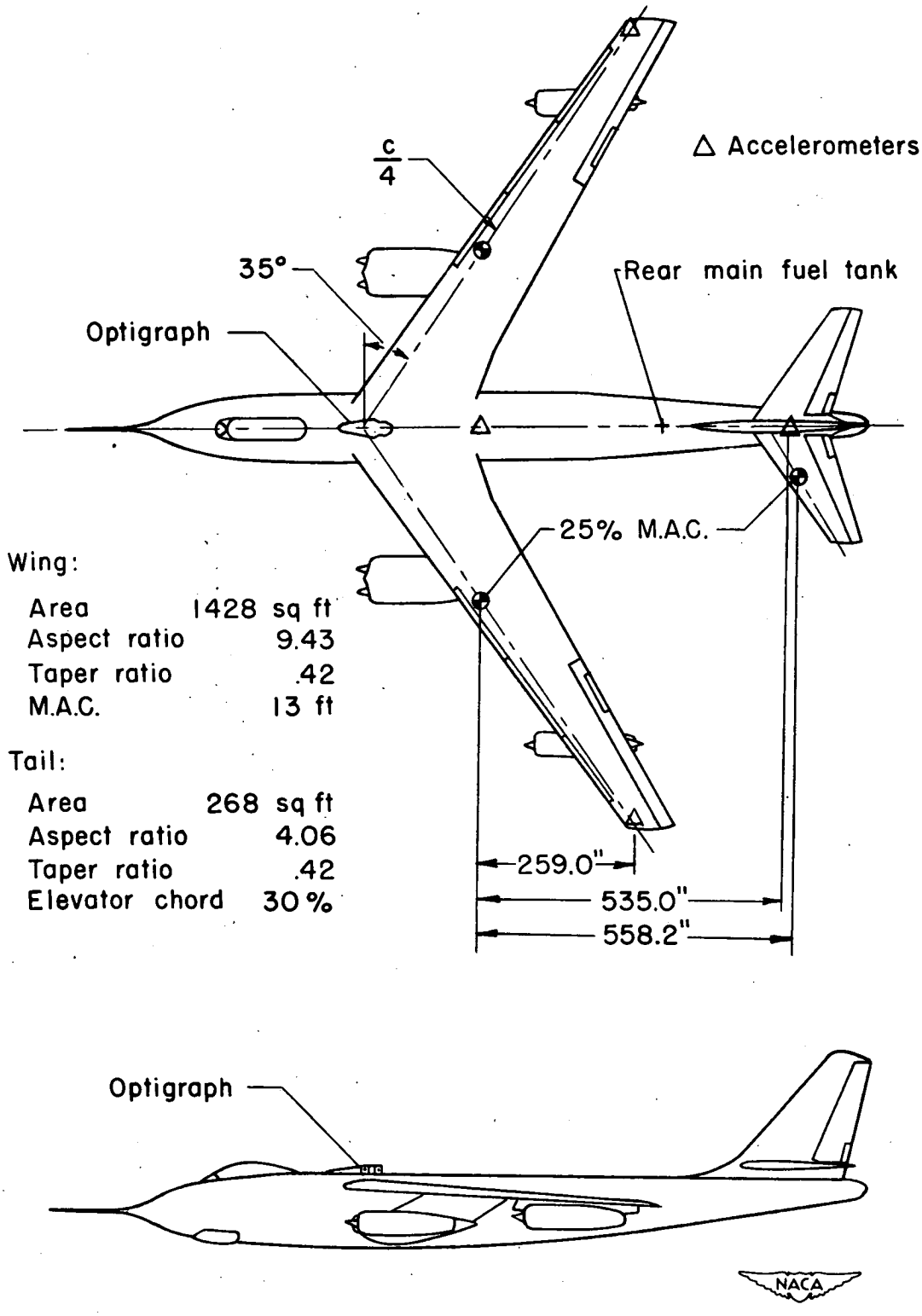

Figure 2.- Two-view drawing of test airplane.

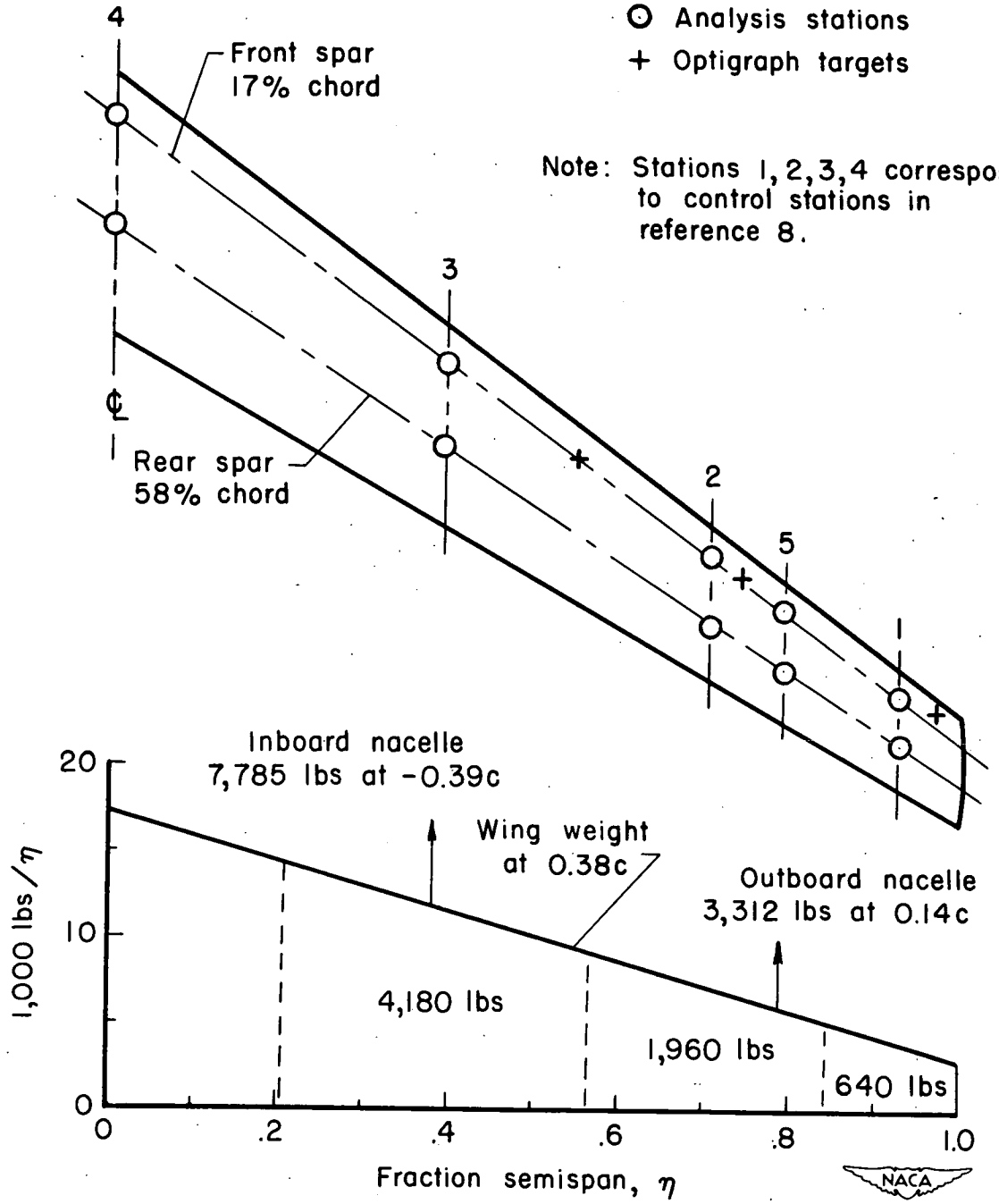

Figure 3.- Wing stations and weight distribution used in analysis.

[redacted]

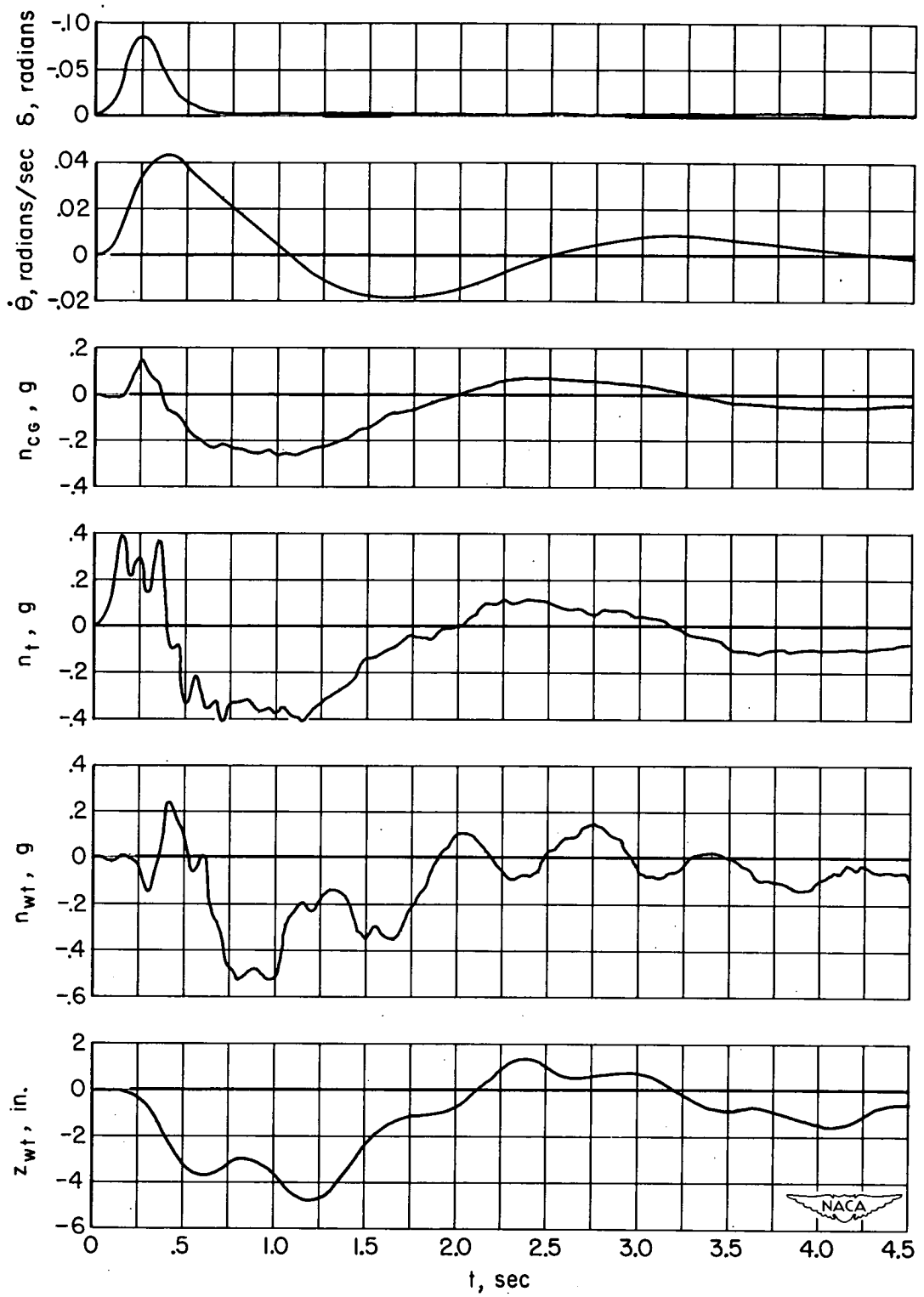

Figure 4.- Typical time histories of input and output response quantities.

[redacted]

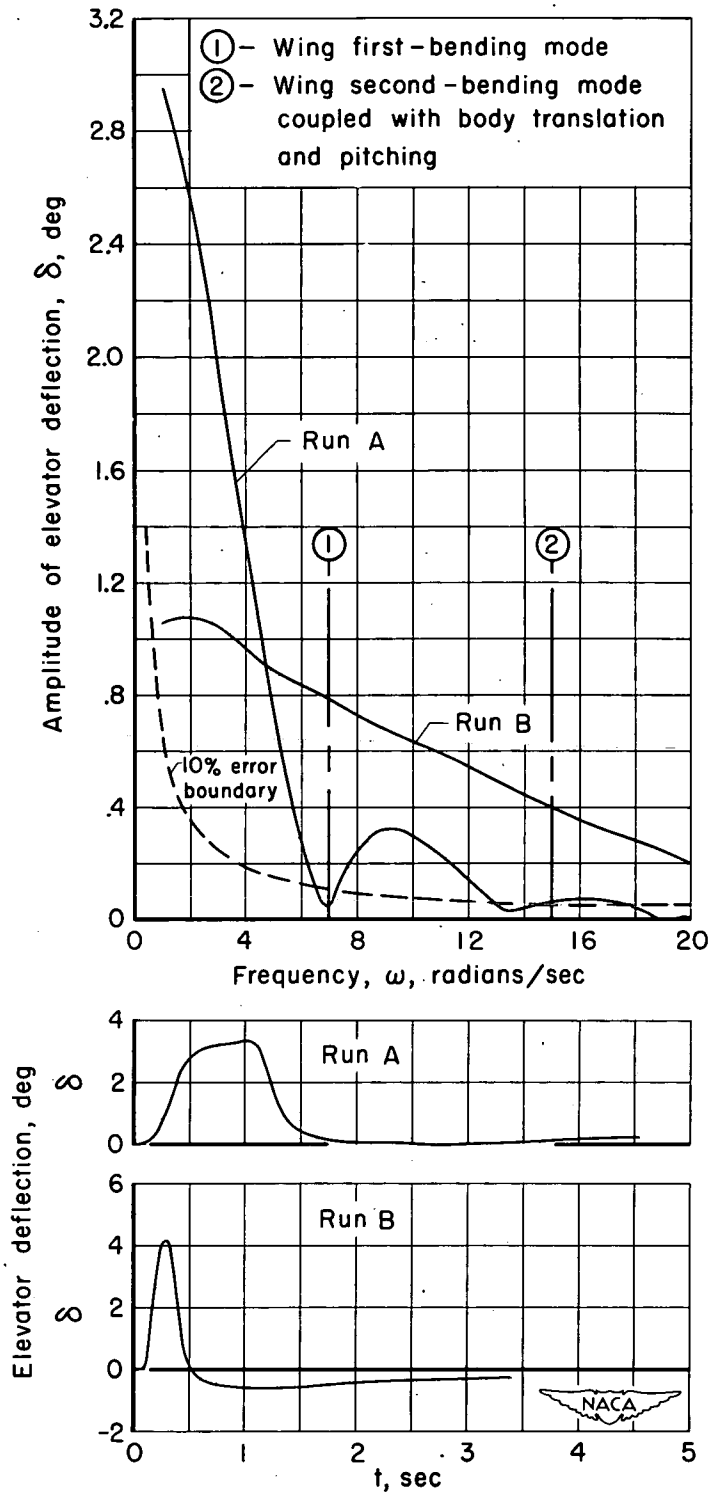

Figure 5.- Typical elevator control inputs and the amplitude of their Fourier transforms.

[redacted]

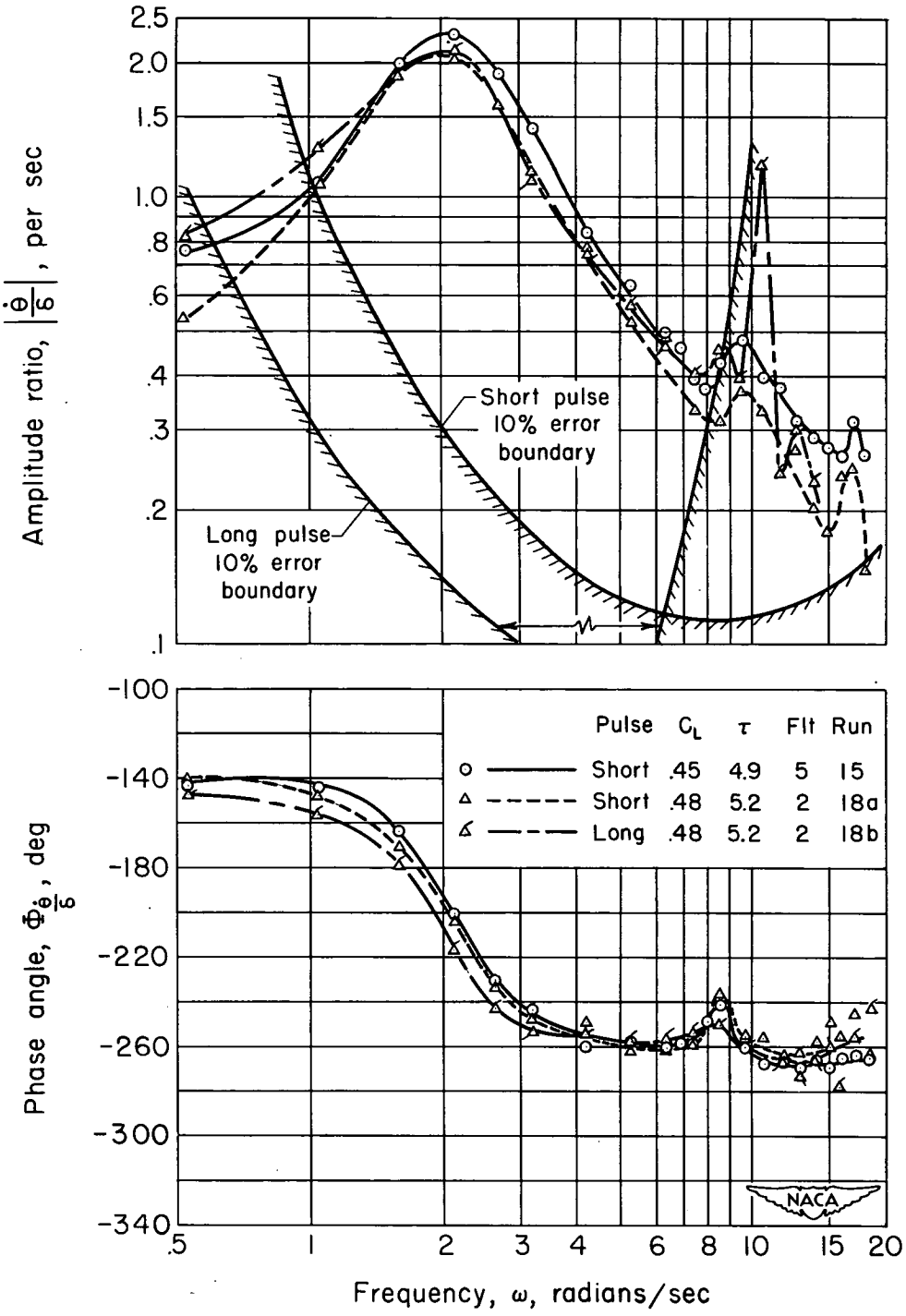

Figure 6.- Comparison of pitching-velocity frequency responses obtained from a long- and a short-pulse elevator input at the same flight condition and from a short-pulse input at a slightly different flight condition; M = 0.72.

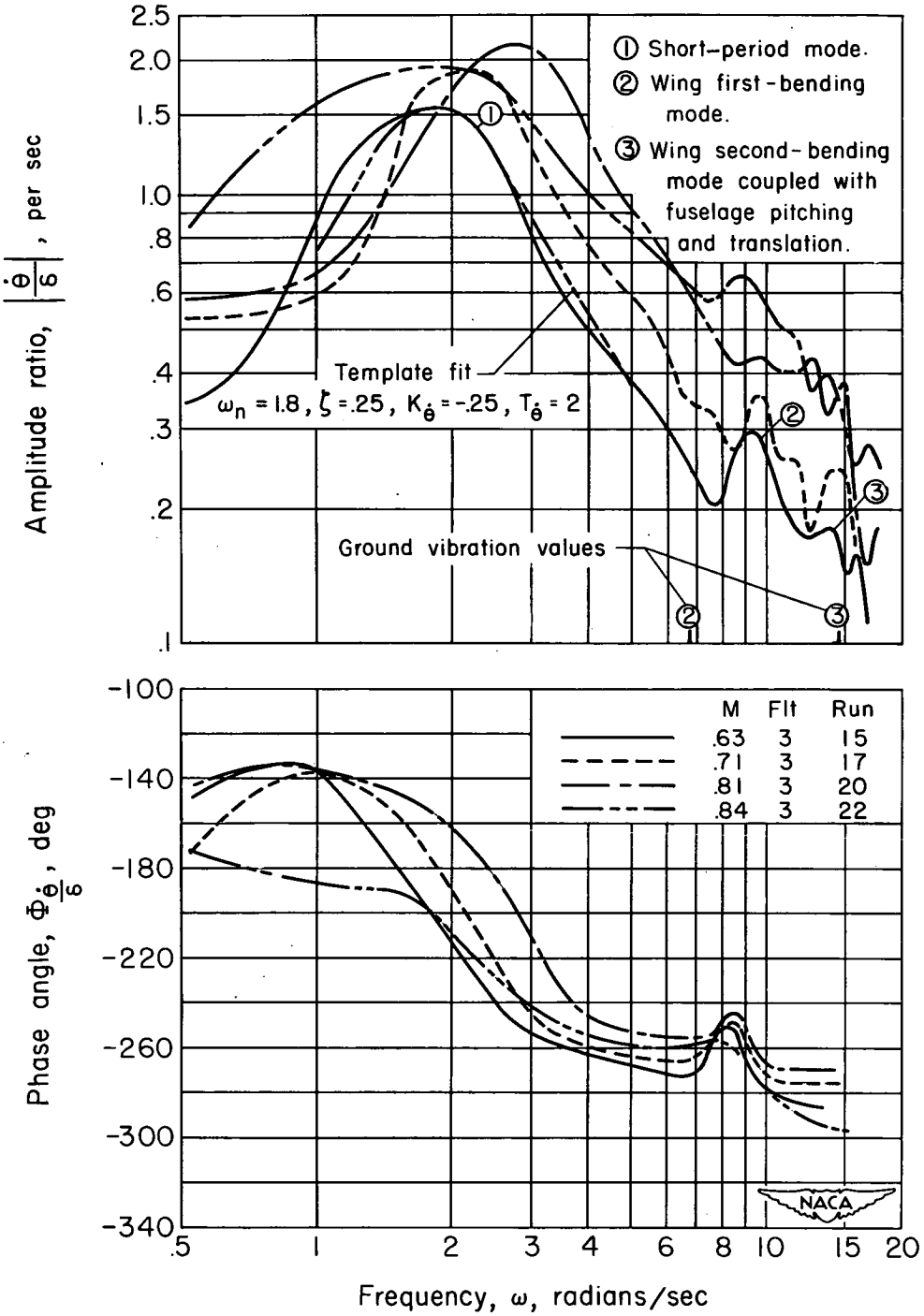

(a) Pitching velocity at the center of gravity.

Figure 7.- Frequency response for the center of gravity at approximately 12.5 percent $\bar{c}$.

[redacted]

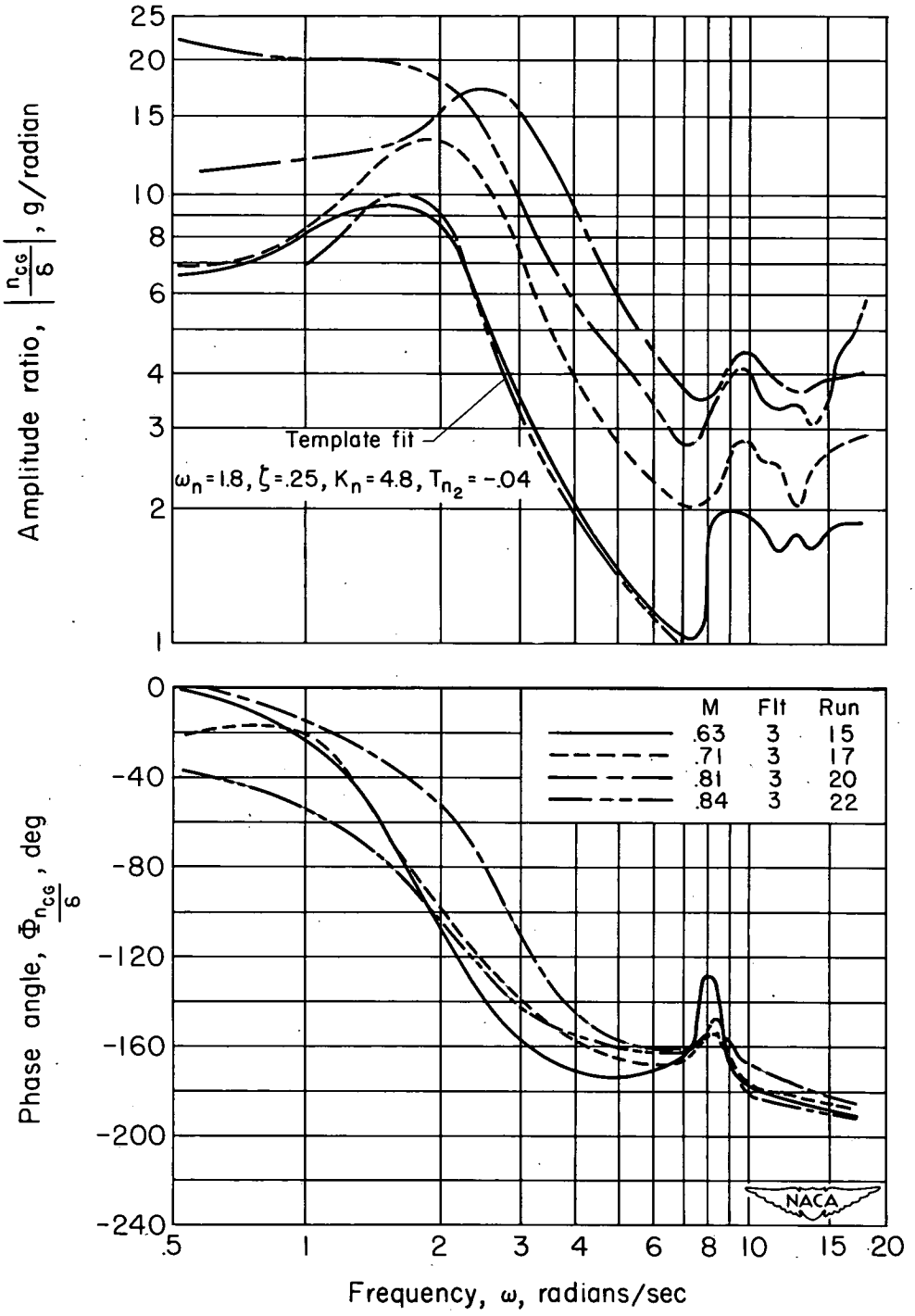

(b) Acceleration at the center of gravity.

Figure 7.- Continued.

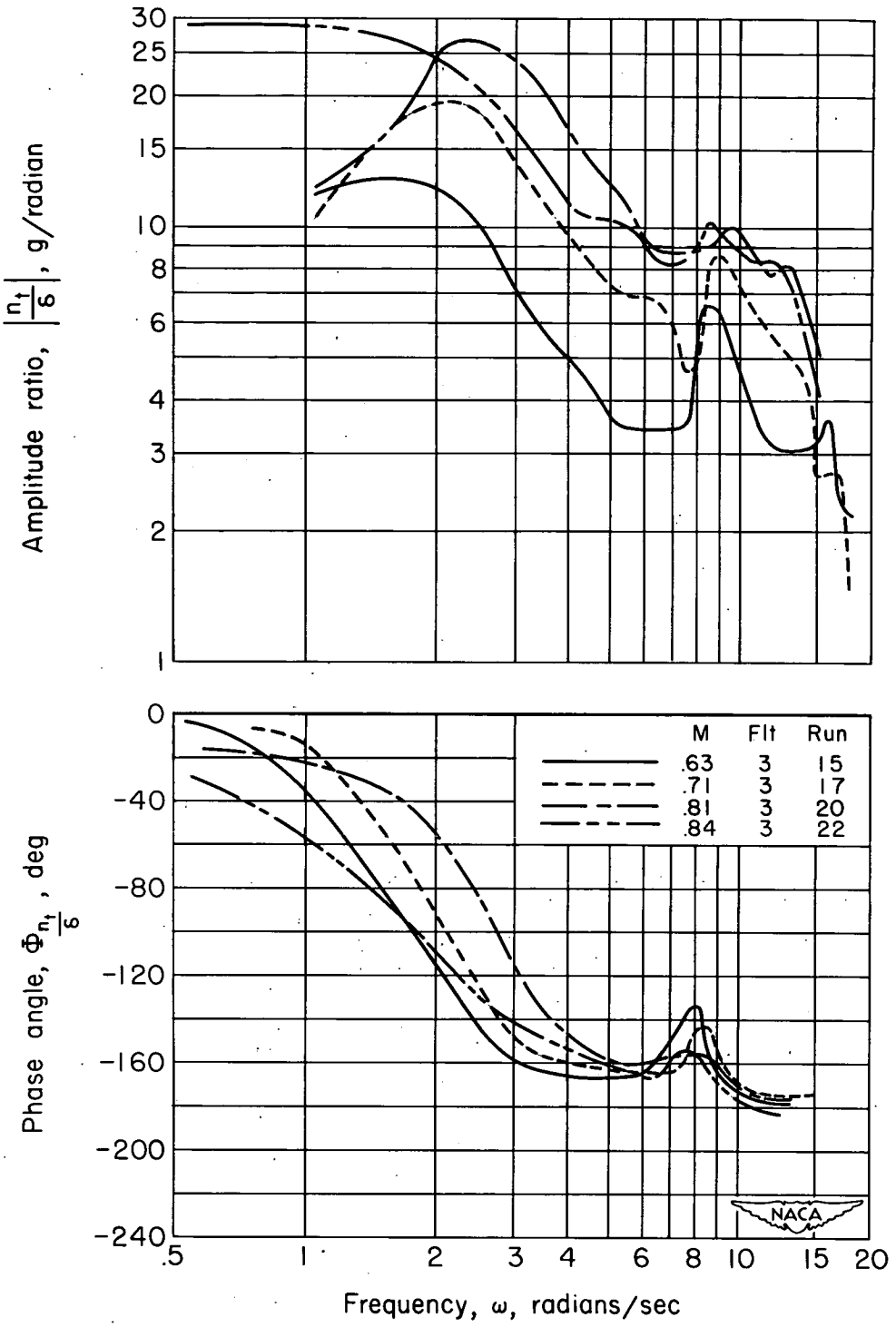

(c) Acceleration at the tail.

Figure 7.- Continued.

[redacted]

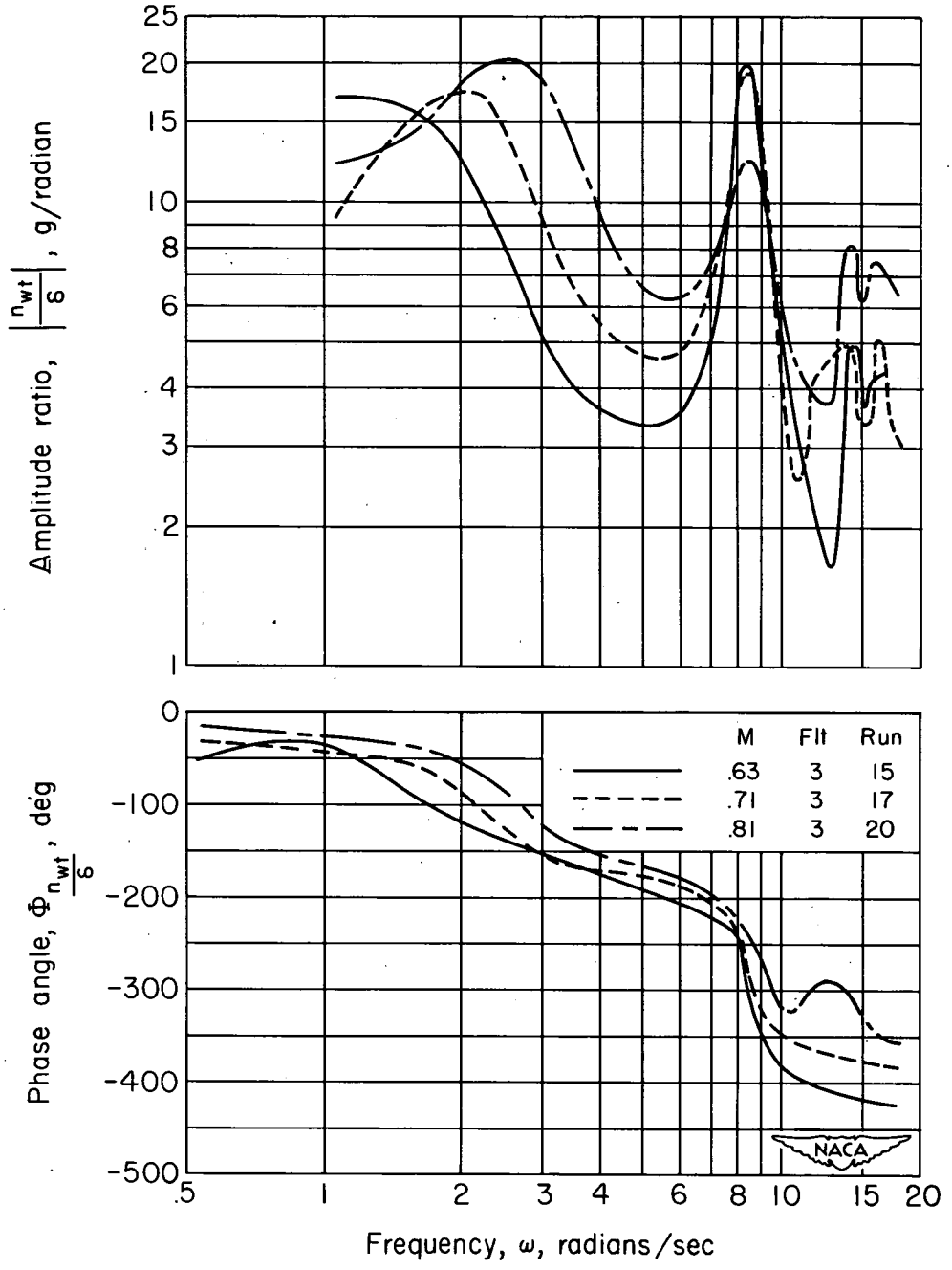

(d) Acceleration at the wing tip.

Figure 7.- Concluded.

[redacted]

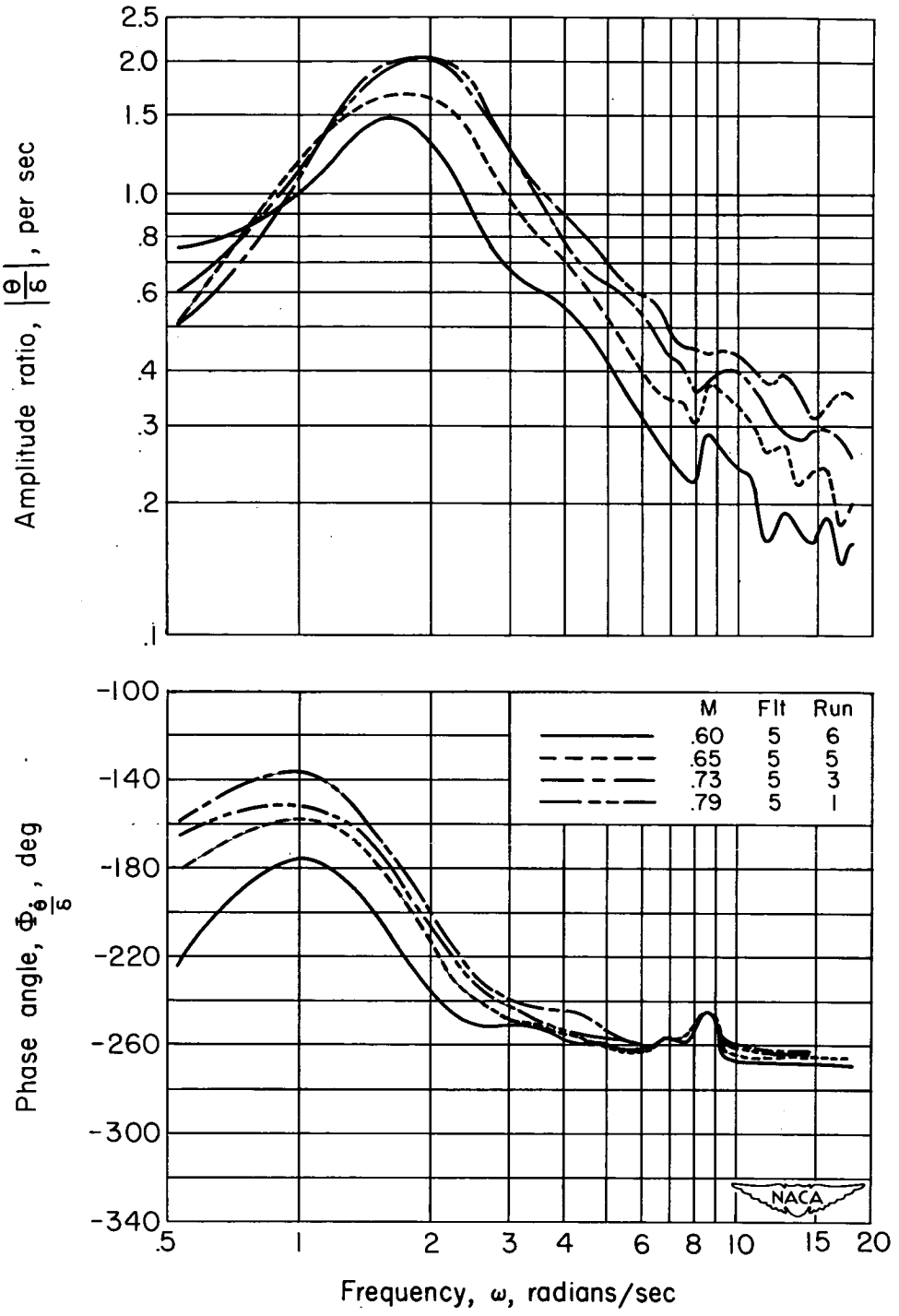

(a) Pitching velocity at the center of gravity.

Figure 8.- Frequency response for the center of gravity at approximately 25-percent $\bar{c}$.

[redacted]

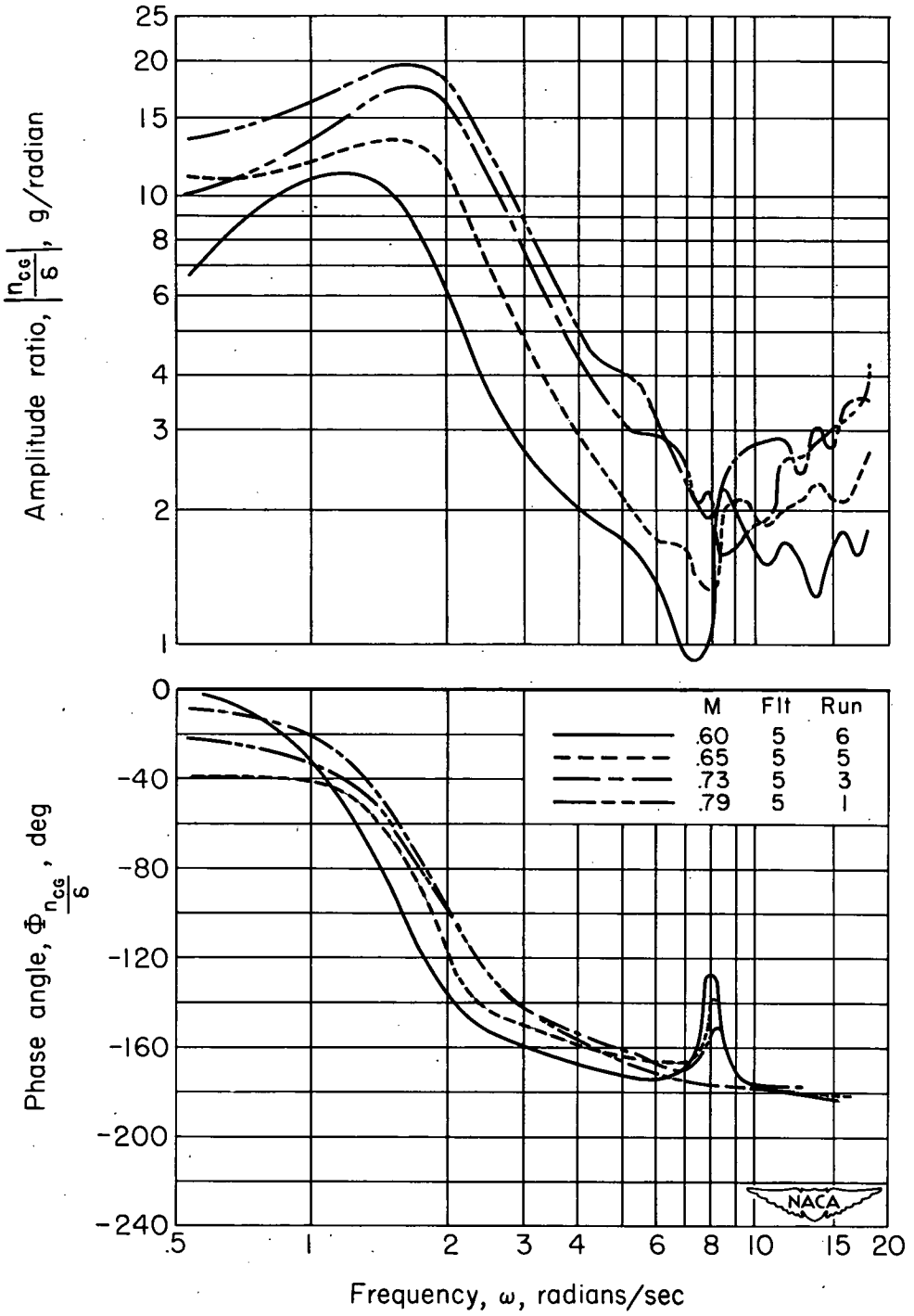

(b) Acceleration at the center of gravity.

Figure 8.- Continued.

[redacted]

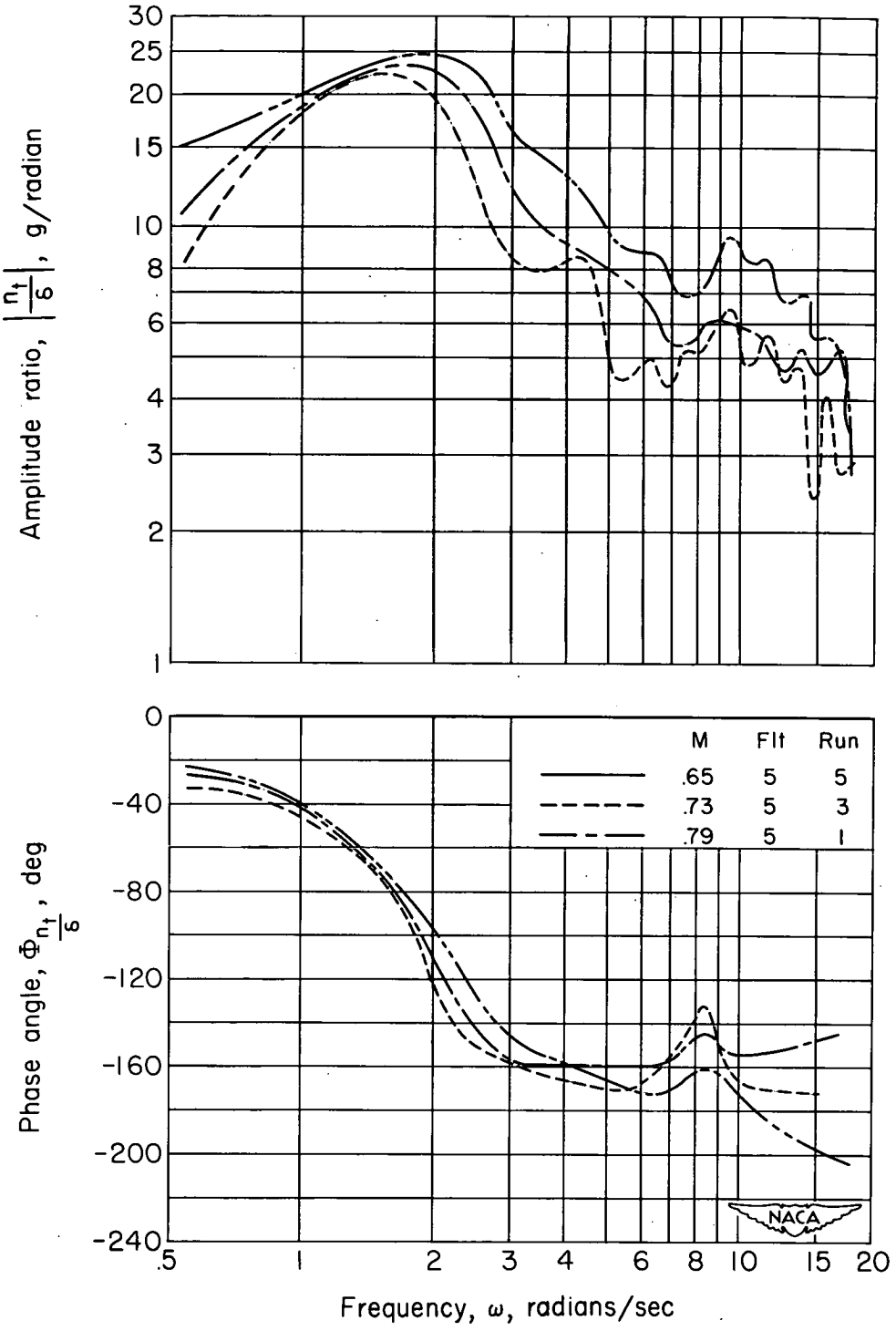

(c) Acceleration at the tail.

Figure 8.- Continued.

[redacted]

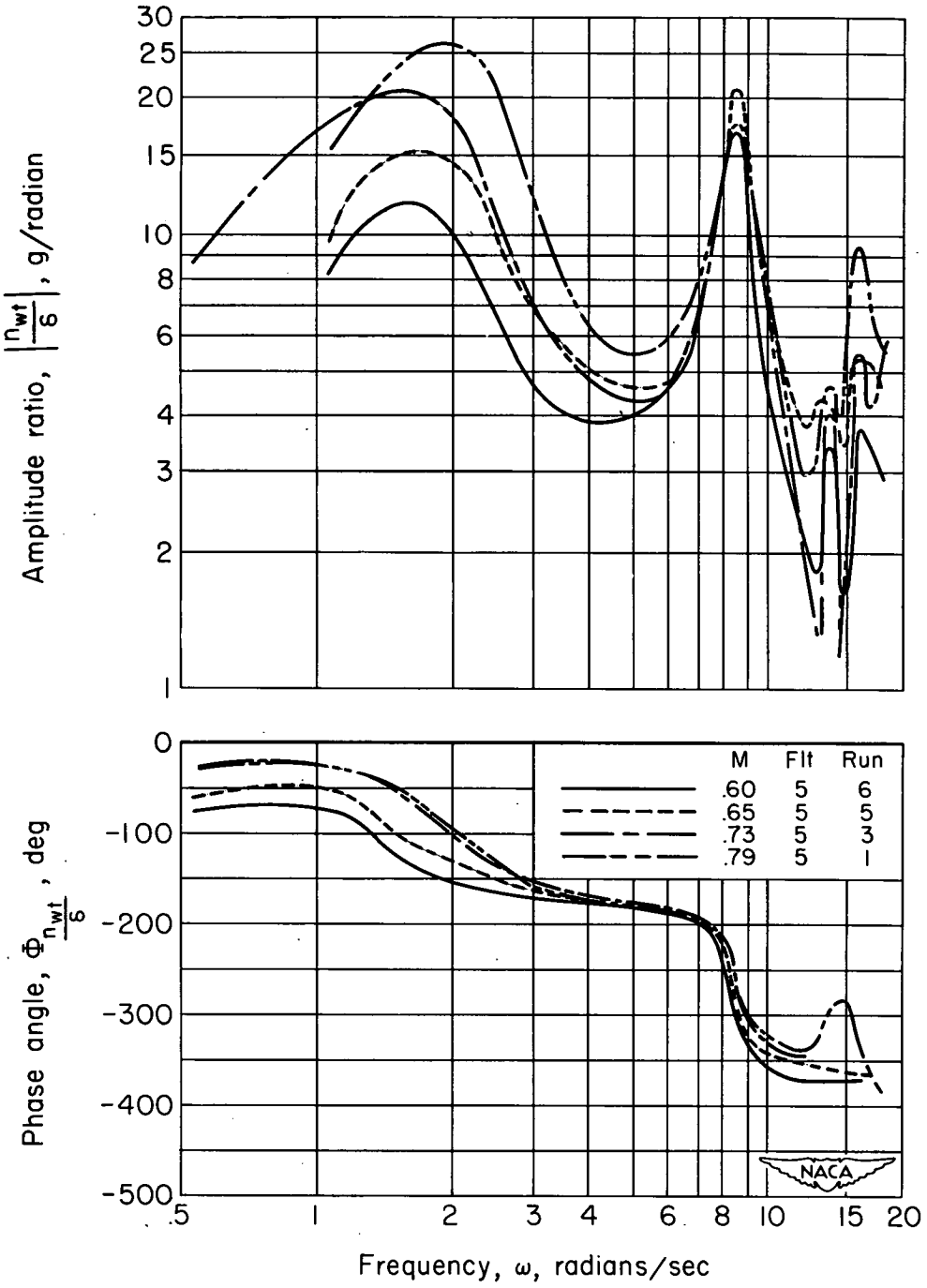

(d) Acceleration at the wing tip.

Figure 8.- Concluded.

[redacted]

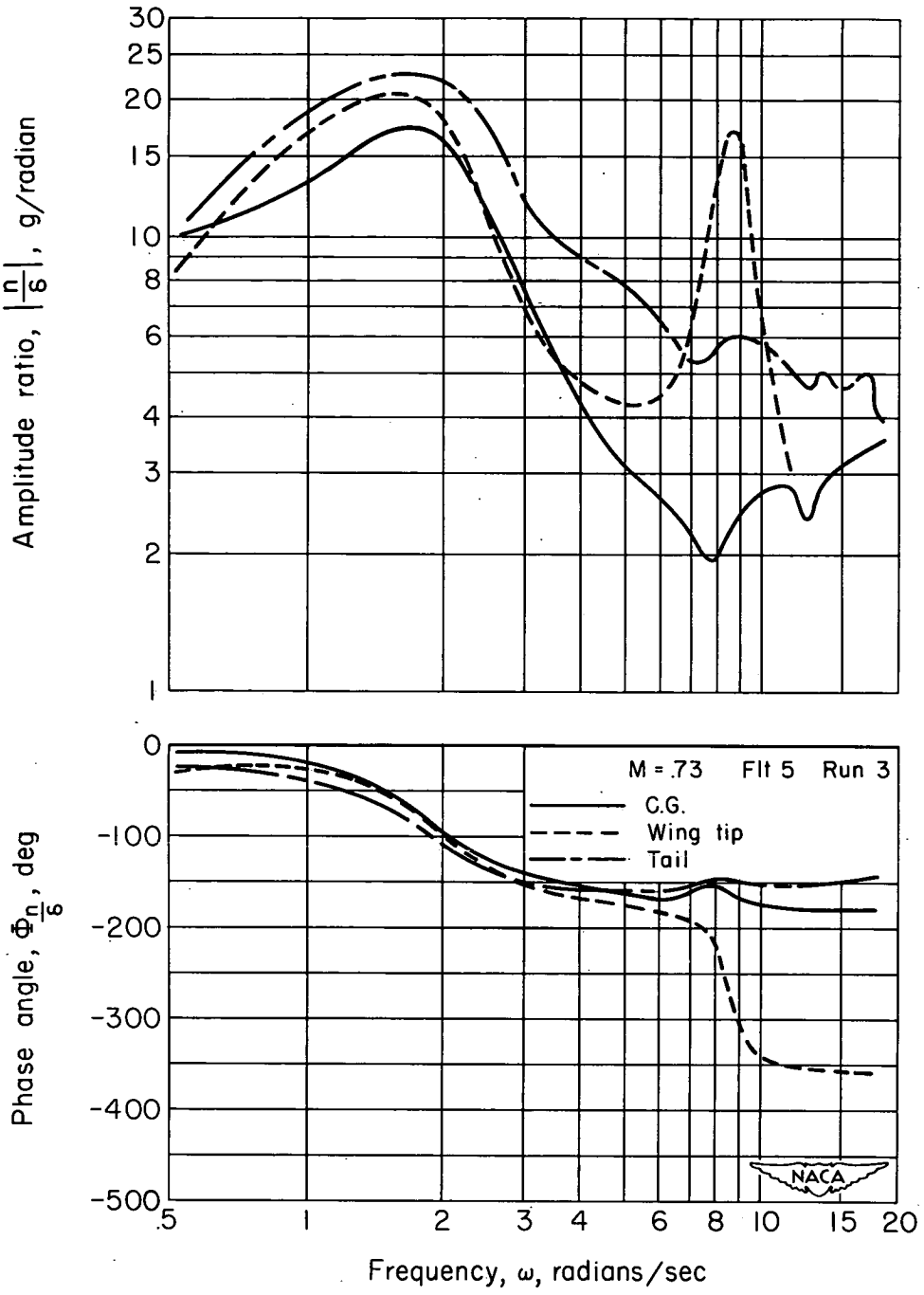

Figure 9.- Comparison of acceleration frequency response at several stations on the airplane.

[redacted]

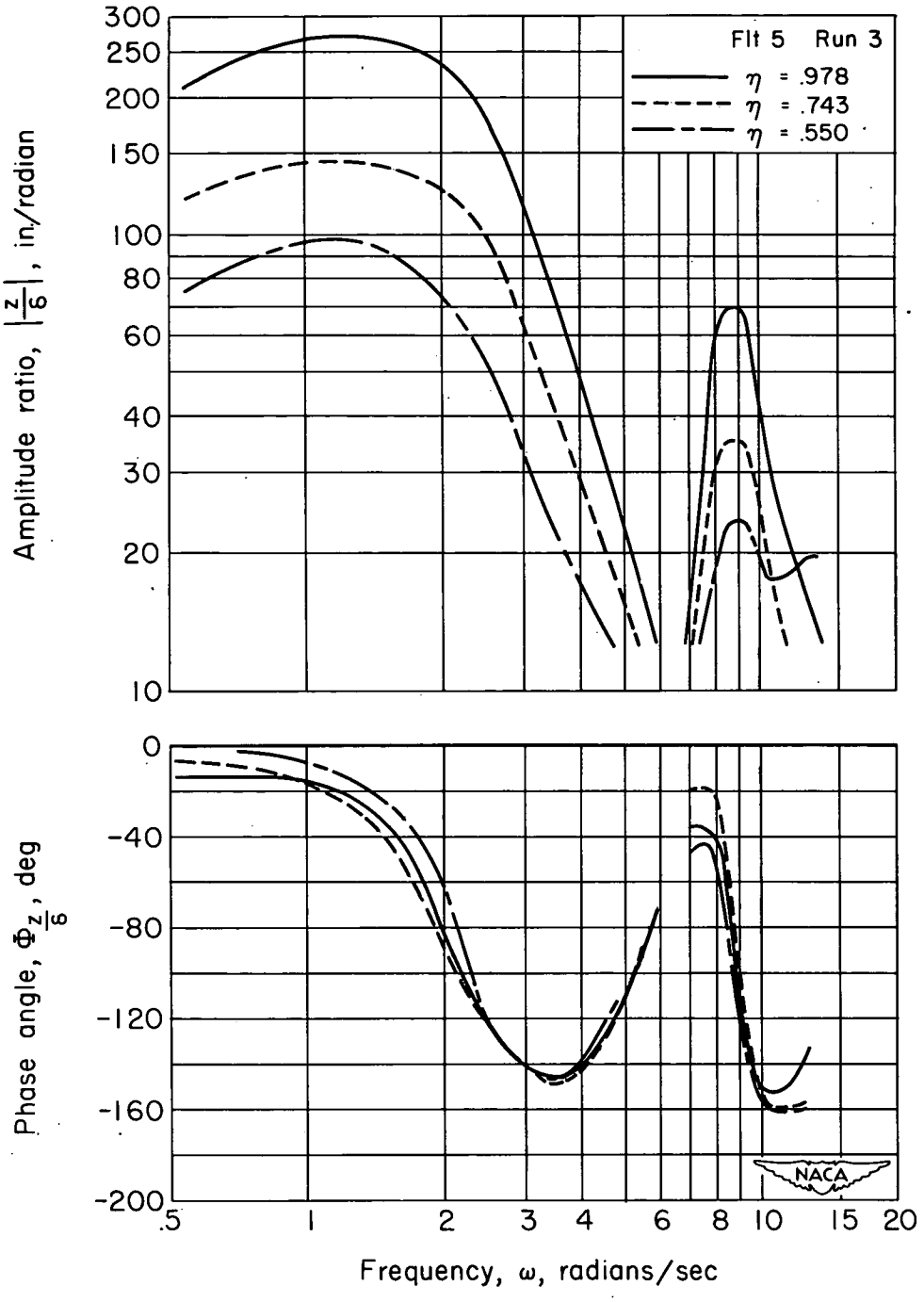

Figure 10.- Wing-deflection frequency response for various spanwise stations.

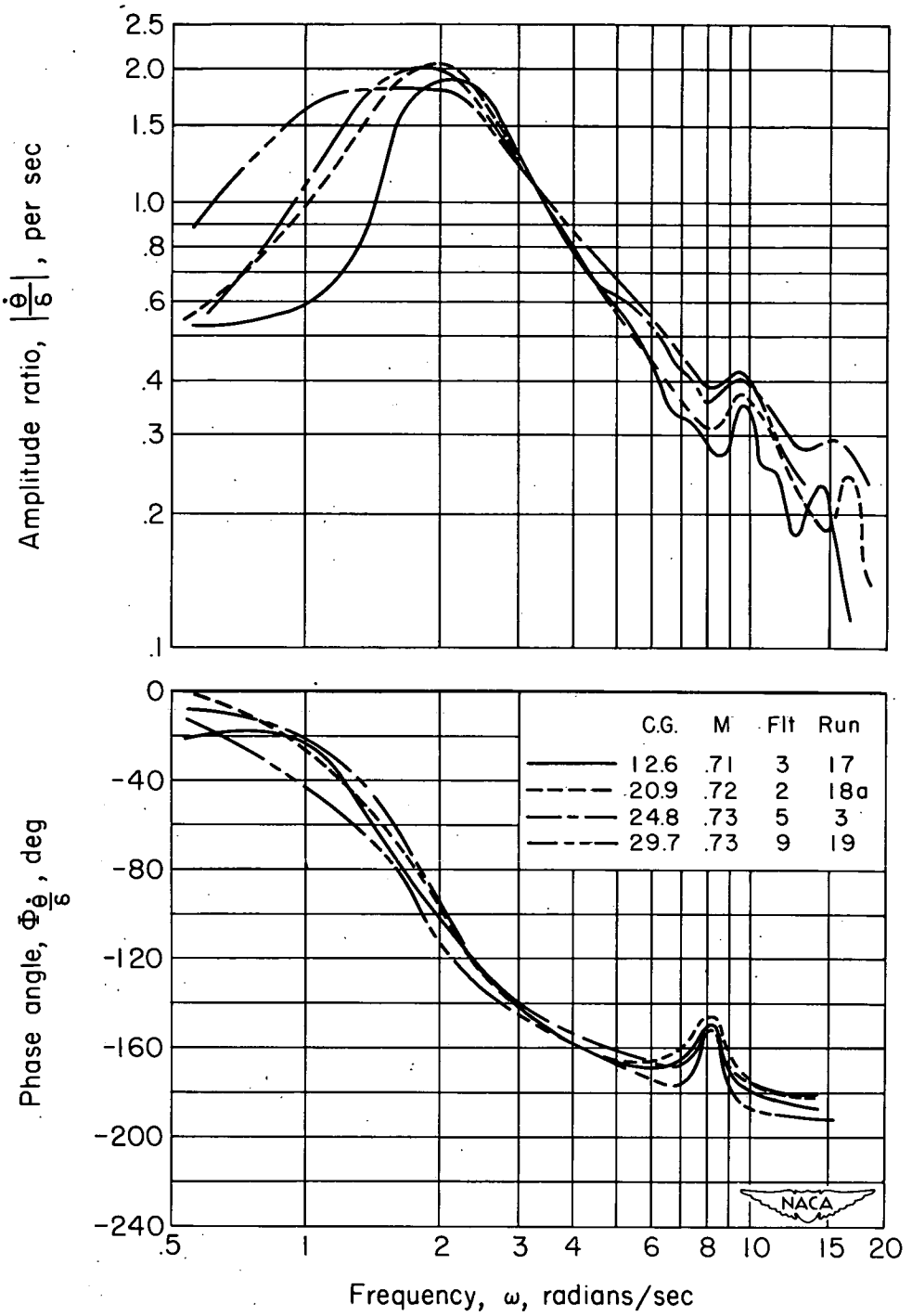

(a) Pitching velocity at the center of gravity.

Figure 11.- Comparison of frequency responses for various center-of-gravity locations for approximately the same flight condition.

[redacted]

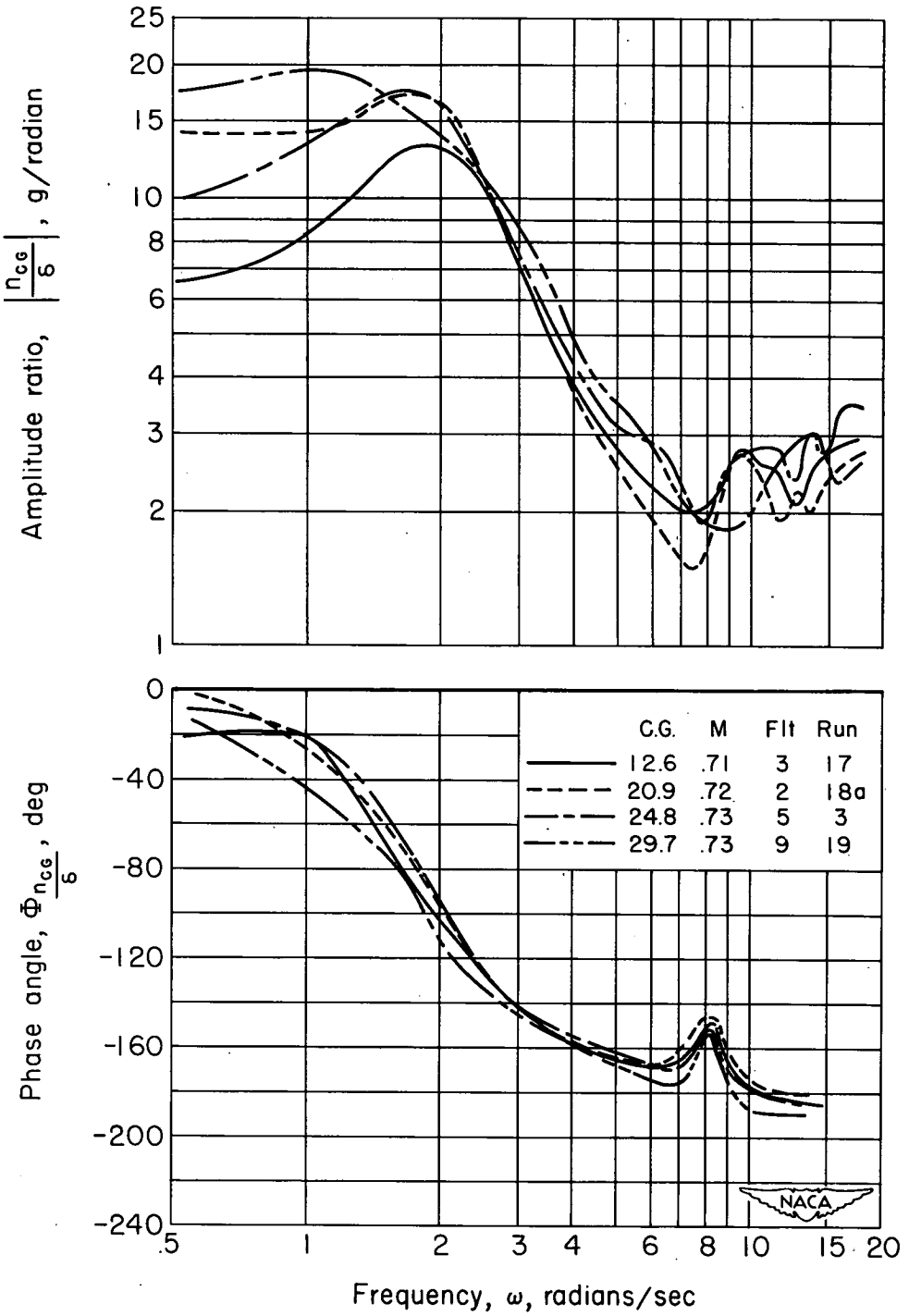

(b) Acceleration at the center of gravity.

Figure 11.- Concluded.

[redacted]

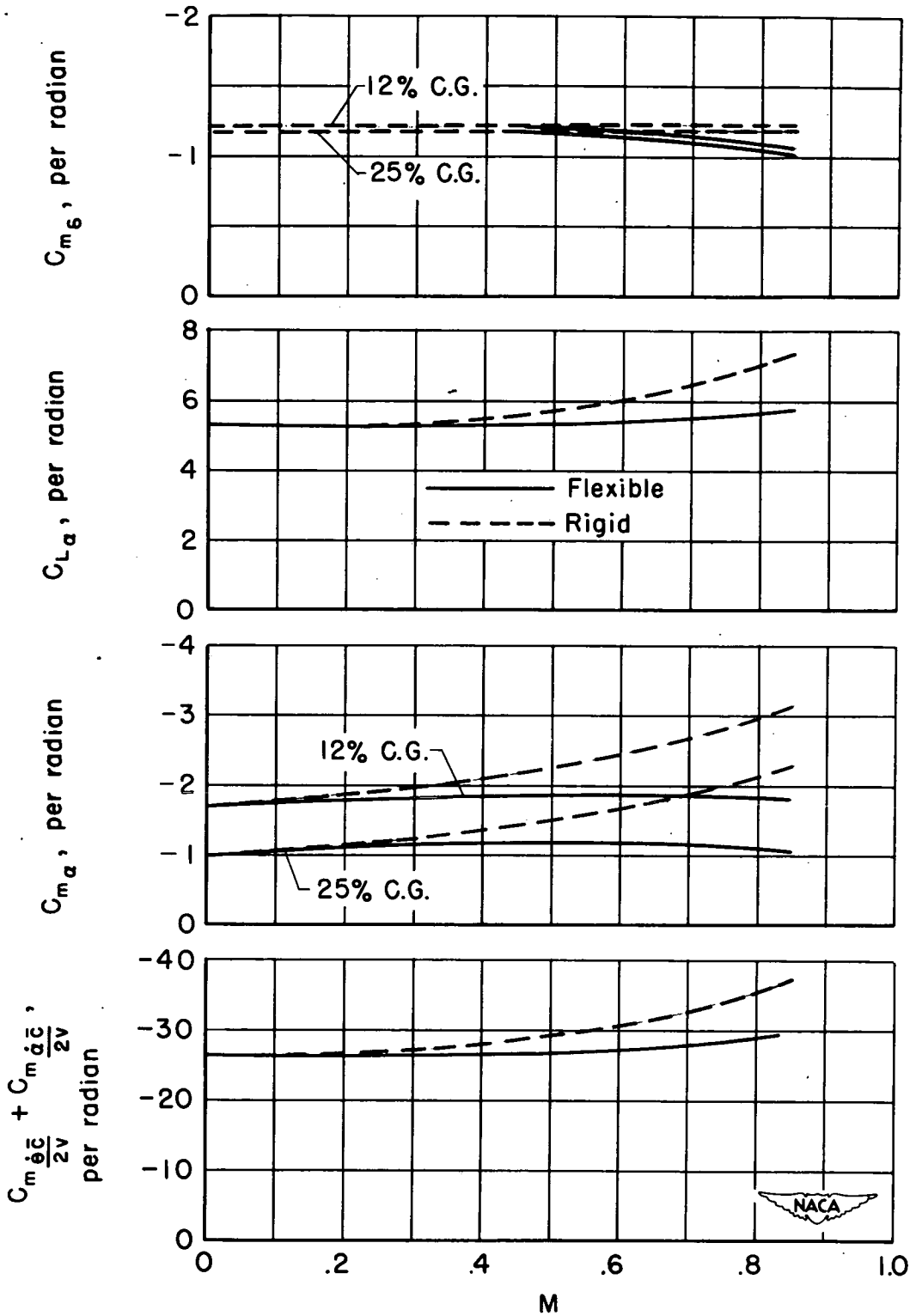

Figure 12.- Predicted effect of flexibility on some of the longitudinal stability derivatives at an altitude of 35,000 feet.

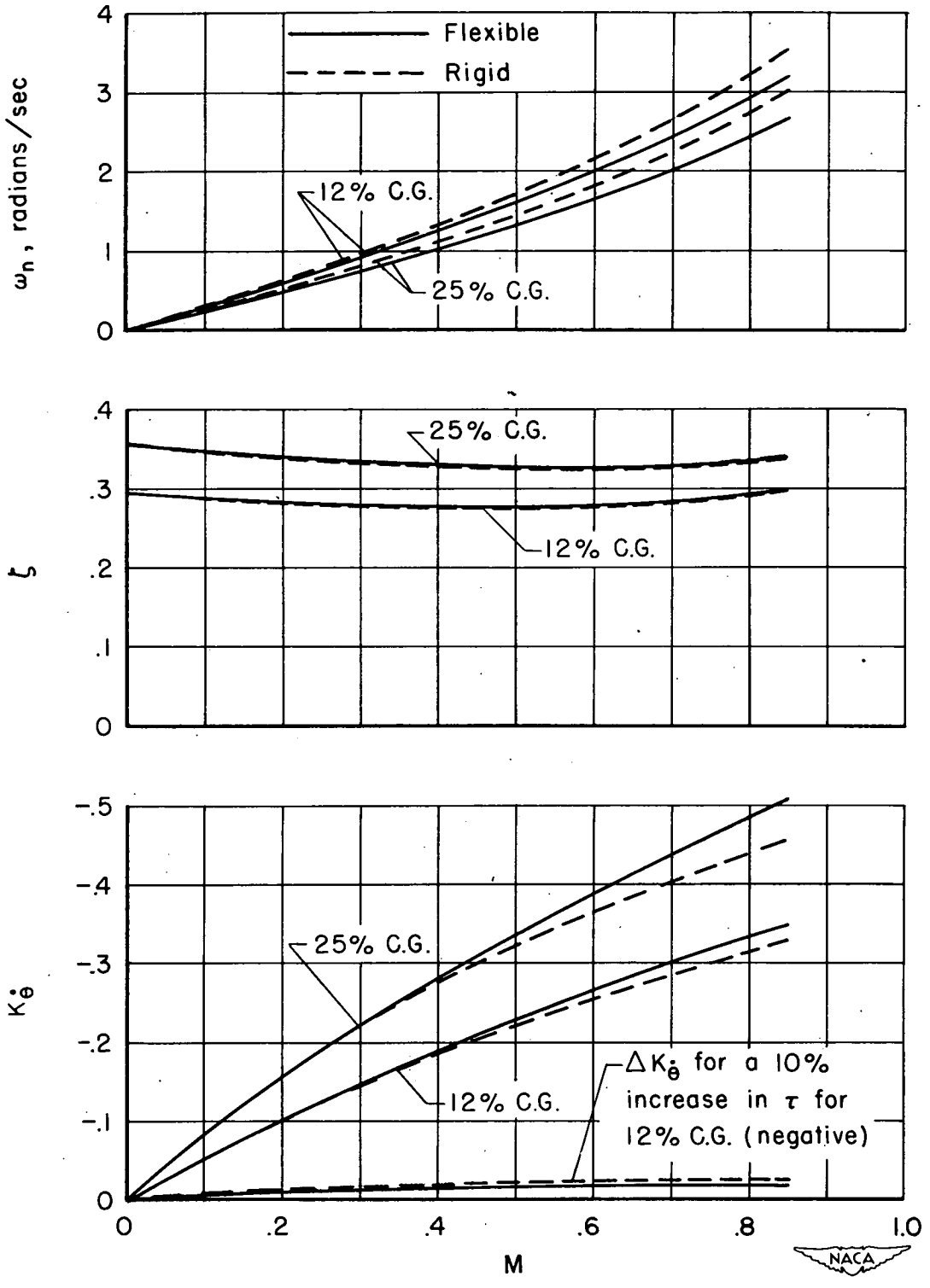

Figure 13.- Predicted transfer-function coefficients at an altitude of 35,000 feet; W = 100,000 pounds, K_Y^2 = 2.4.

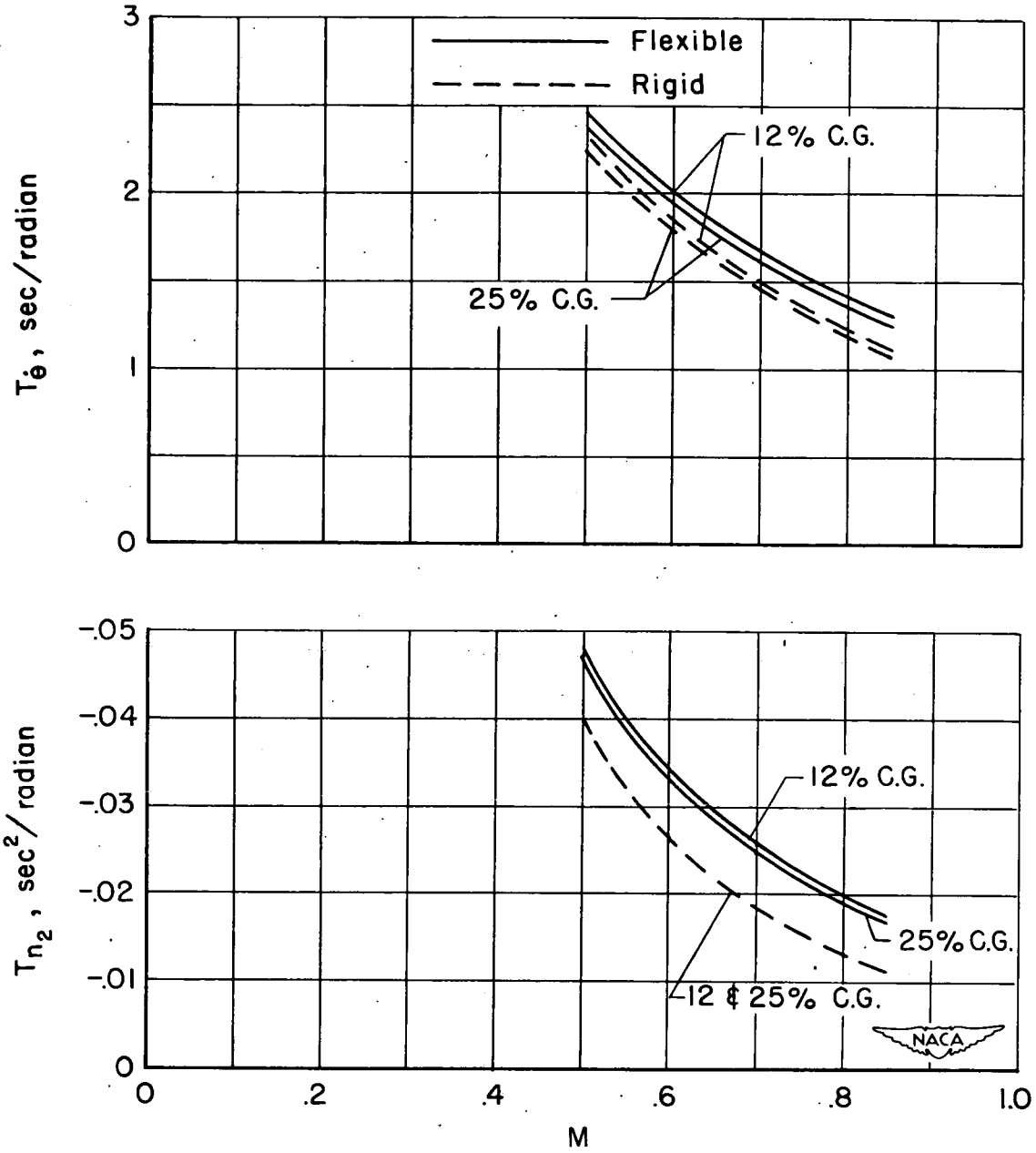

Figure 13.- Concluded.

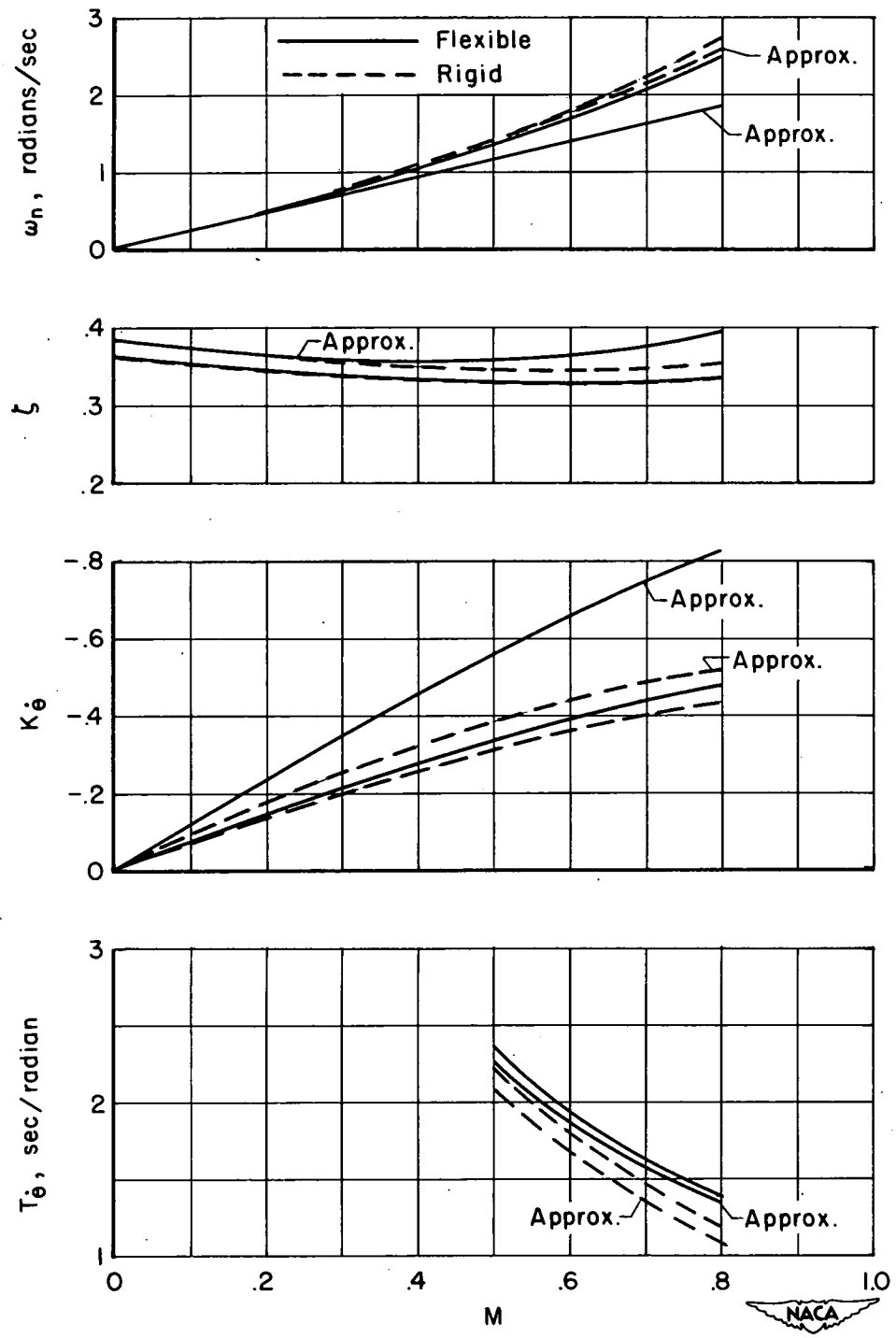

Figure 14.- Comparison of transfer-function coefficients calculated from the approximate equations with those from the complete equations for the flexible and the rigid airplane; W = 100,000 pounds, c.g. = 25-percent M.A.C.

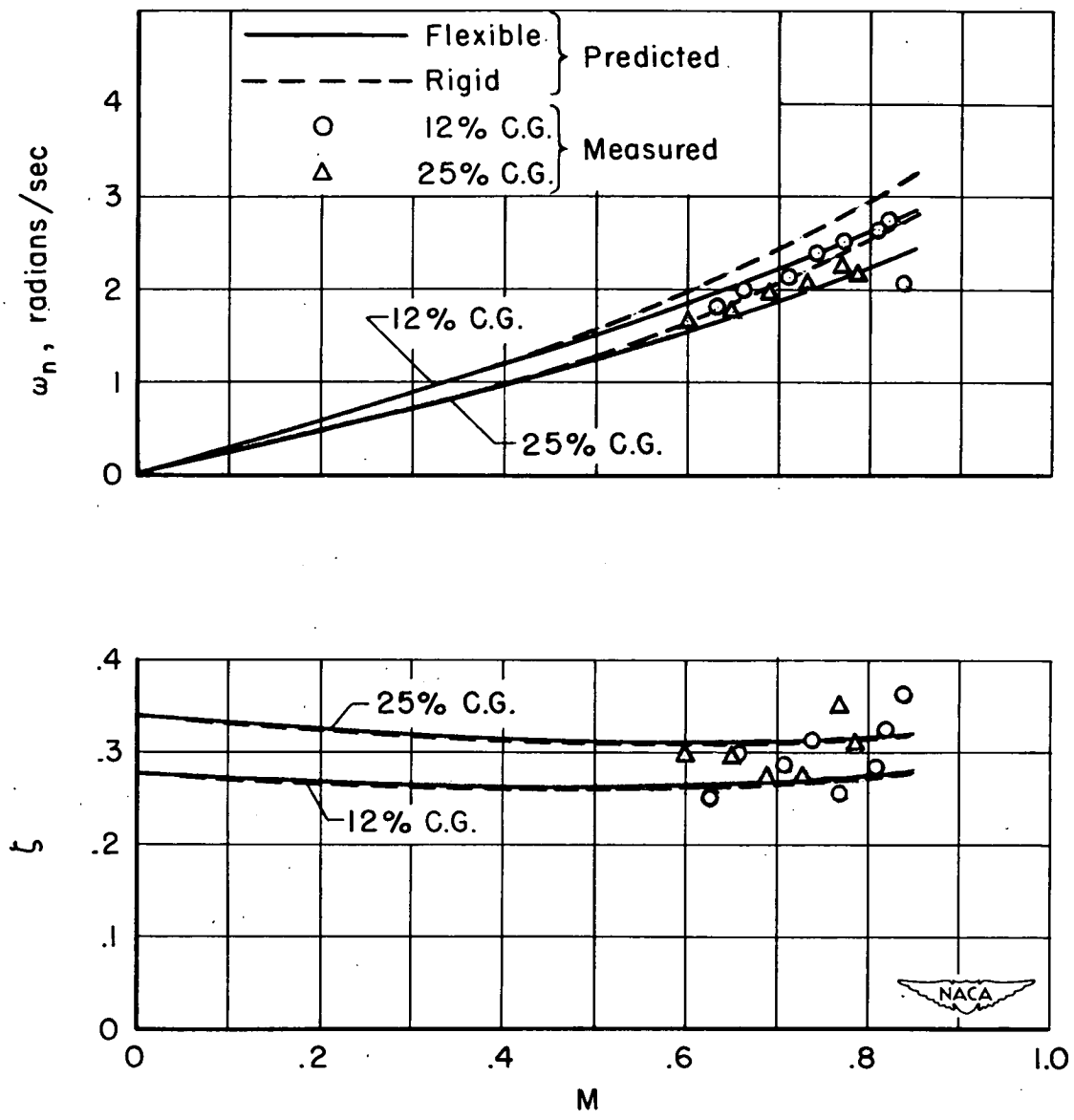

Figure 15.- Comparison of predicted and experimental values of transfer-function coefficients; W = 115,000 pounds.

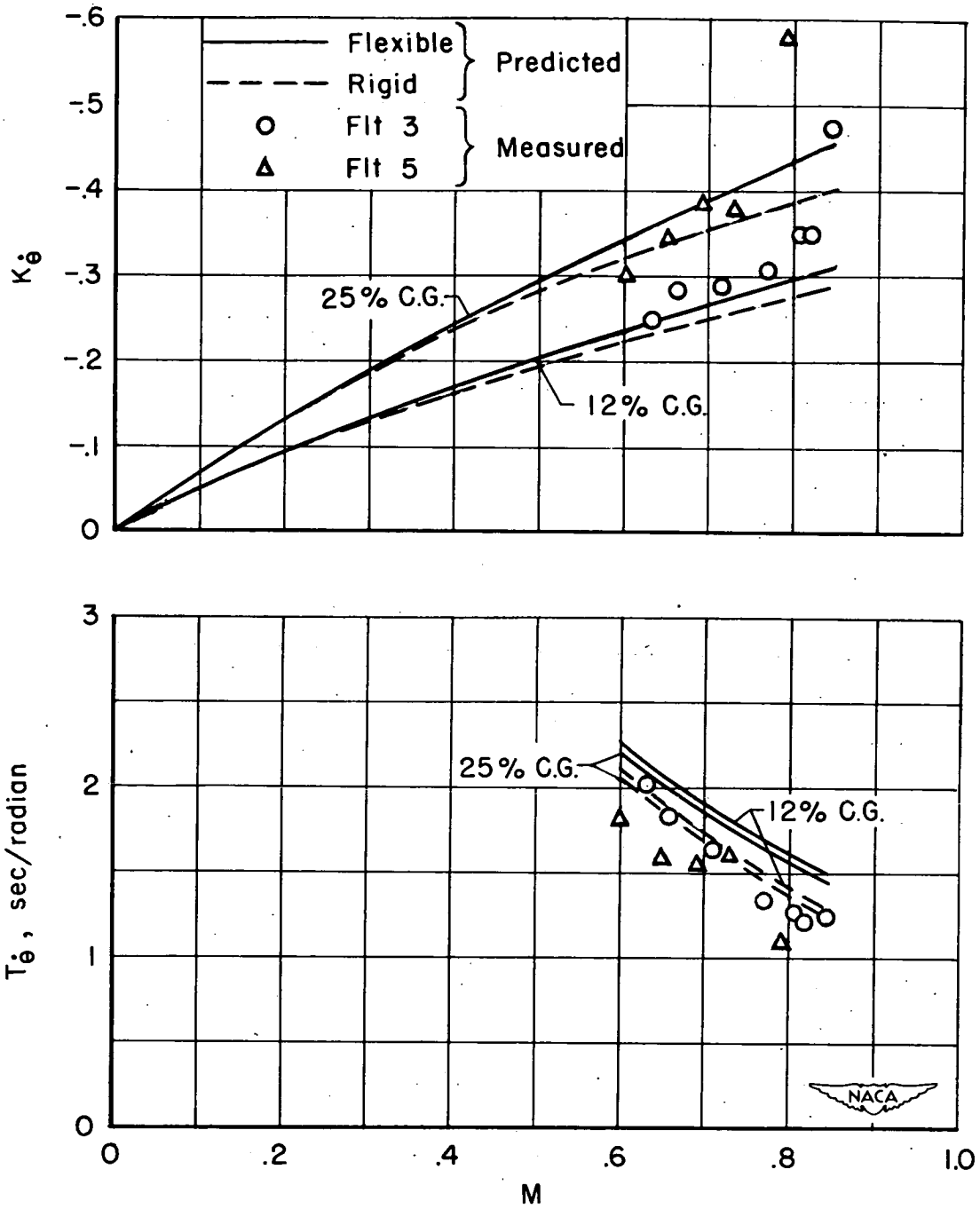

Figure 15.- Concluded.

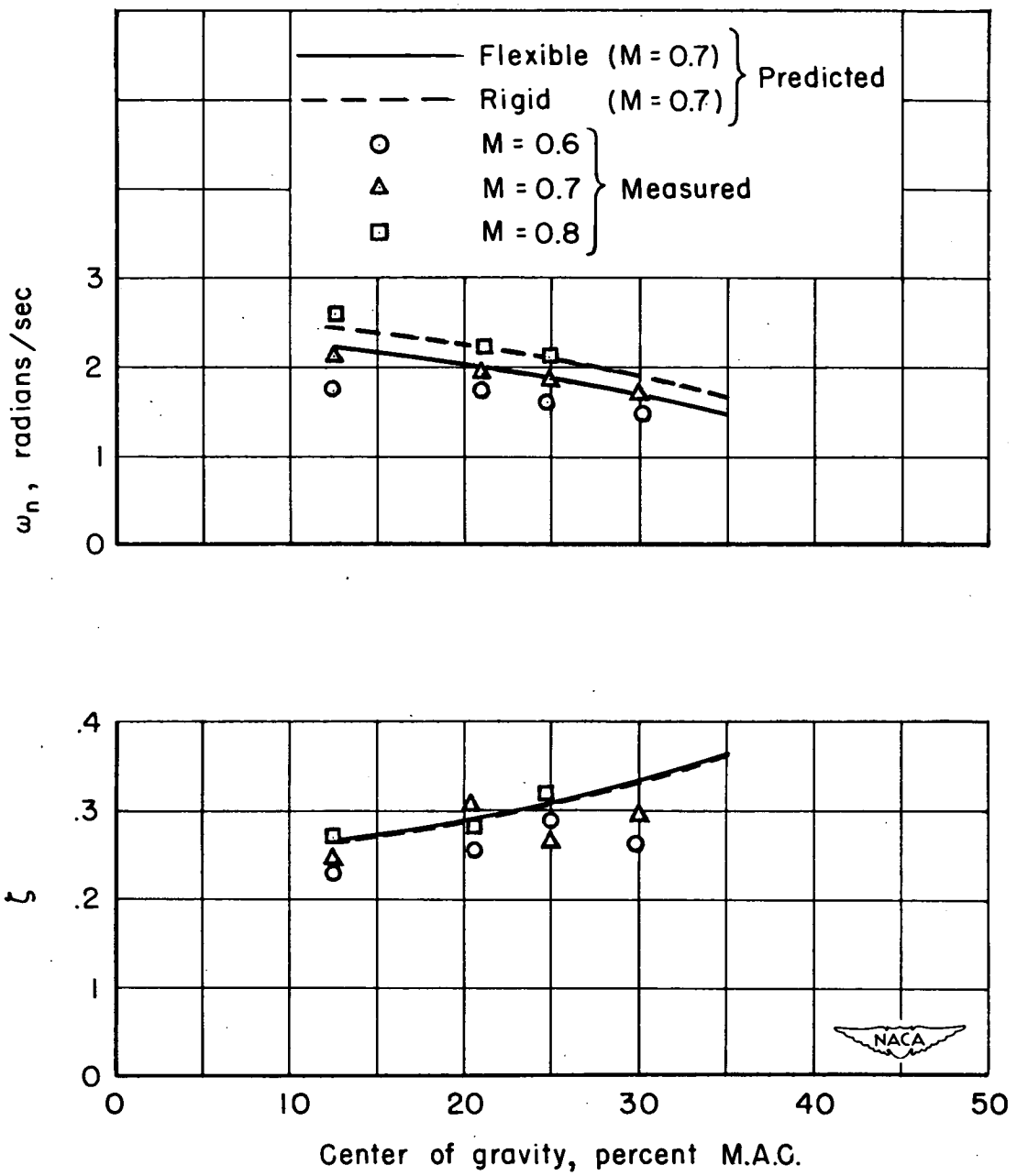

Figure 16.- Comparison of predicted and experimental variation with center-of-gravity position of natural frequency and damping ratio of the short-period mode; W = 115,000 pounds.

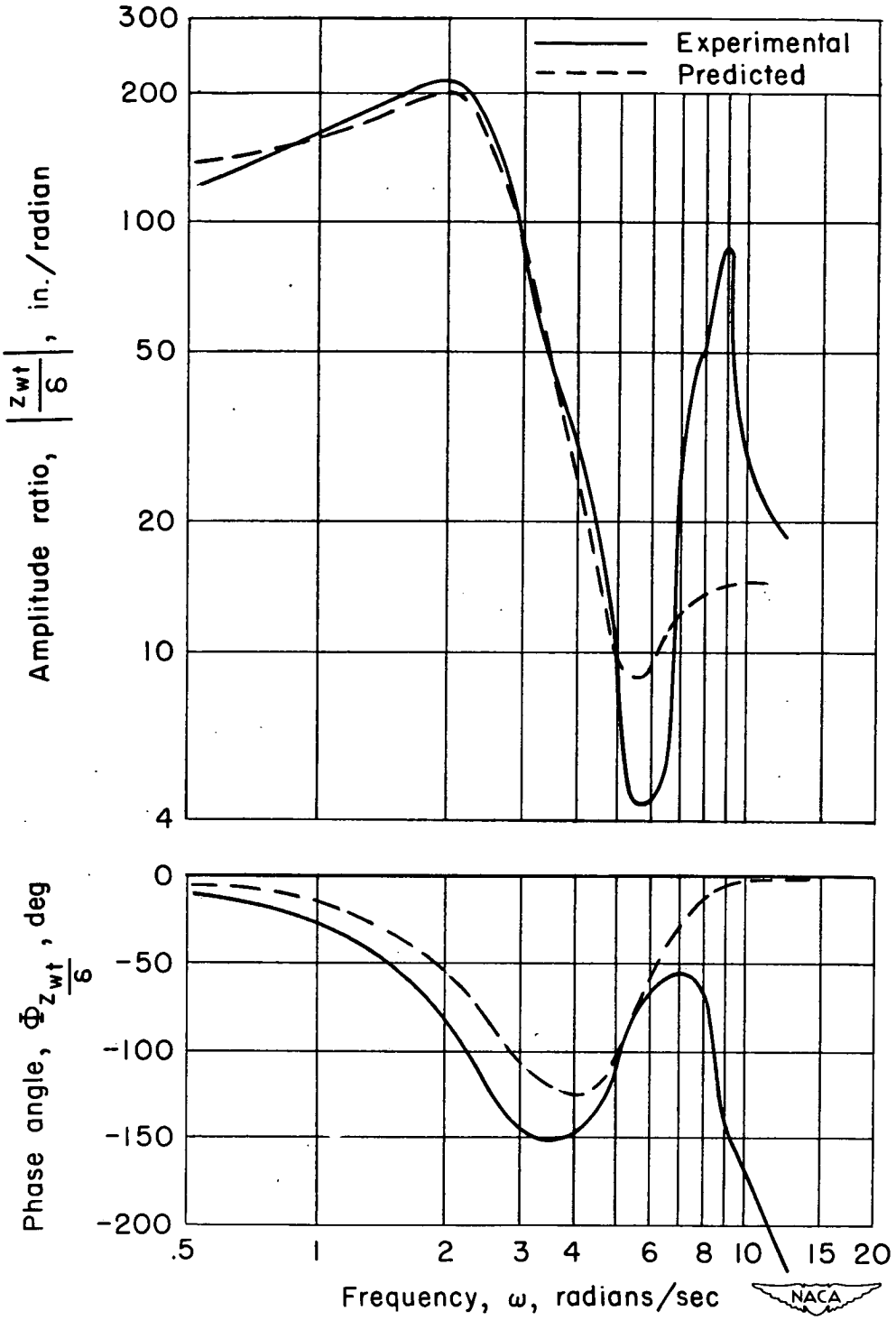

Figure 17.- Comparison of experimental and predicted wing-tip-deflection frequency response for Flight 3, Run 17.

NACA-Langley - 11-26-54 - 300